Glacial ice impacts: Part II: Damage assessment and ice-structure interactions in accidental limit states (ALS)

Zhaolong Yu [a,b,1,*], Wenjun Lu [c,d,e], Marnix van den Berg [c,d], Jørgen Amdahl [a,b], Sveinung Løset [c,d]

[a] Department of Marine Technology, Norwegian University of Science and Technology (NTNU), Norway
[b] Center for Autonomous Marine Operations and Systems (AMOS), Norwegian University of Science and Technology (NTNU), Norway
[c] Sustainable Arctic Marine and Coastal Technology (SAMCoT), Norwegian University of Science and Technology (NTNU), Norway
[d] ArcISo AS, Trondheim, Norway
[e] The Norwegian Academy of Science and Letters, DNVA, Oslo, Norway

ABSTRACT

Floating glacial ice features of various sizes pose a substantial threat to the structural integrity of offshore structures in ice-prone regions. Relatively small ice feathers, e.g., bergy bits and growlers, are a major concern because they are more difficult to detect by marine radars and perform concurrent ice management operations, especially in extreme sea states.

This two-part companion paper aims to assess potential loads of accidental ice actions that are exerted on an offshore semi-submersible platform and the consequences of these actions. Paper I investigates the probability distributions of glacial ice impact velocities and the associated impact heights under different sea states. Given the critical impact energy identified from Paper I, Paper II investigates ice crushing and structural damage during glacial ice impacts in accidental limit states (ALS) and ice-structure interactions. Three different approaches, i.e., the integrated approach, weakly coupled approach and fully coupled approach, are employed. The methods are based on different coupling strategies between ice and the structure and are used to identify the critical local ice sharpness for stiffened panels of the platform column, which causes maximum structural damage given an energy demand. The accuracy of the simulation results, calculation efficiency and scope of application using the three approaches are compared and discussed.

With the identified critical sharpness of the ice model, numerical simulations are performed to impact various locations of the platform column. Apart from scenarios with head-on ice impacts, several oblique impact scenarios are simulated, where the glacial ice feature slides along the contact plane with different initial indentations of the panel. The results are discussed with respect to the resistance and energy absorption of the ice and structure and ice-structure interactions.

1. Introduction

Floating offshore structures in ice-prone regions are exposed to potential threats from glacial ice impacts. Glacial ice features of

---

* Corresponding author. Department of Marine Technology, Norwegian University of Science and Technology (NTNU), Norway.
E-mail address: zhaolong.yu@ntnu.no (Z. Yu).
[1] ISSC2021 committee member, V1. Accidental Limit States.

Abbreviations

|	
ALS	Accidental Limit States
BWH criterion	Bressan-Williams-Hill criterion
DEM	Discrete Element Method
IACS	International Association of Classification Societies
ISO	International Organization for Standardization
NLFEA	Nonlinear Finite Element Analysis
P-A relationship	Pressure - Area relationship
PC3	Polar Class 3
SAMS	Simulator for Arctic Marine Structures
ULS	Ultimate Limit States
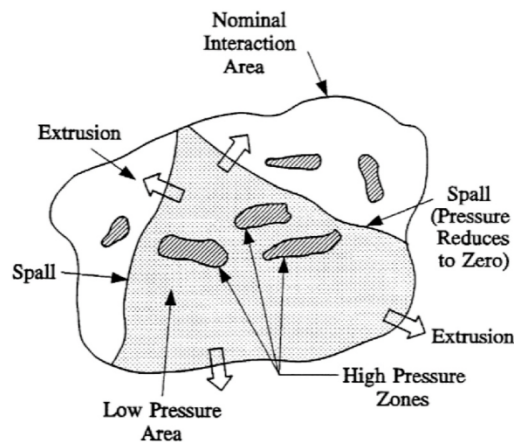
Fig. 1. Definition of the nominal contact area and the actual contact area, from Jordaan [3].

various sizes driven by environmental loads, such as waves, currents and winds, may collide with the platform and cause severe structural damage, economic loss and fatalities. For safety considerations, it is crucial to understand the structural response and ice-structure interactions during accidental glacial ice collisions and thus enables proper design of structures against such abnormal actions. The term 'ice' in the paper specifically refers to 'glacial ice features' unless otherwise defined.

In the design of structures, limit states methodologies are often employed by engineering communities and classification societies. ISO-19906 [1] specifies that the characteristic values for actions that arise from ultimate limit states (ULS) and accidental limit states (ALS) should be determined based on an annual probability of exceedance not greater than 10^{-2} and 10^{-4}, respectively. The principles for the ULS and ALS design of ships and offshore structure against ice impacts in polar regions are reviewed by Amdahl [2]. Conventional structural design against ice actions primarily follows the procedure for ULS design, where a structure should be able to resist all foreseeable loads and actions with minor structural damage. The procedure for ULS design is generally based on linear elastic methods for structural analysis or plastic methods that correspond to moderate yielding. In the ULS design of structures, the ice resistance is often represented by the pressure area (P-A) relationship $p = C \cdot A^{ex}$, where p is the ice pressure, A is the nominal contact area, and C and ex are empirical coefficients. For glacial ice feature interactions, the nominal contact area is defined as the projected contact area of the ice feature on the surface of the undeformed structure for a given penetration into the ice as shown in Fig. 1. The actual ice pressure distribution is highly nonuniform with several low- and high-pressure zones and possible spalling and extrusion of ice. The actual contact area is the sum area of the low- and high-pressure zones. In view of the complicated ice material properties, the P-A relationship is simple to use, and the ice resistance data for fitting of the pressure curve can be directly obtained from various model tests and full-scale measurements. Structures designed in accordance with the ULS procedures are supposed to be assessed further with ALS ice collisions. However, guidelines from established rules that dictate how this analysis should be performed are incomplete, and relevant research is limited.

In the assessment of structural damage to glacial ice impacts, it is often convenient to decouple the problem into external dynamics and internal mechanics as performed in ship collision analysis. The external dynamics address rigid body motions of the two interacting bodies prior to, during and after a collision. The main outcome of an external dynamic assessment is the energy loss during a collision, which will be dissipated by structural deformation and ice crushing in the assessment of internal mechanics. The internal mechanics assessment of structural deformation under ice loads is often carried out by applying the given ice pressure on the structures. Kõrgesaar et al. [4] studied the overload response of stiffened frames due to ice loading with different patch length and height,
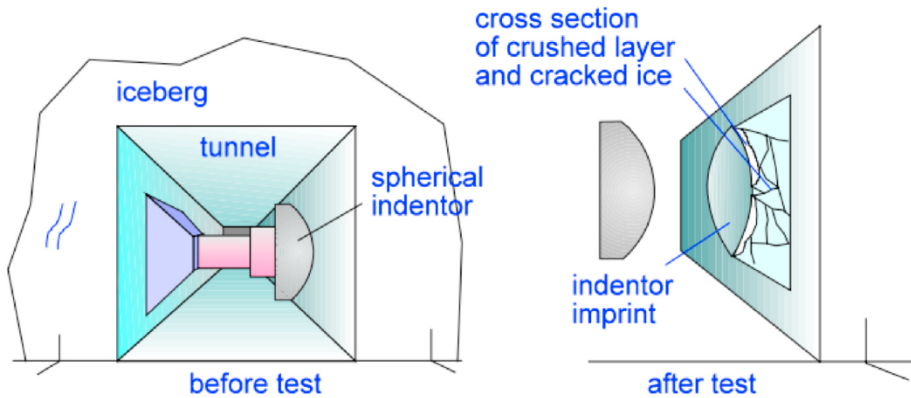
Fig. 2. Arrangement of the Pond Inlet indentation test; picture from Daley [23].

and found that plastic strain localized faster in frames, and shell plating was more sensitive to patch height variations. Yu et al. [5] presented an analytical model for large deformation resistance of an isolated stiffened panel subjected to patch loading considering boundary flexibilities. The model compared well with experiments and numerical simulations, and was well suited for a quick assessment of structural capacities of stiffened panels under ice loading. Daley et al. [6] discussed the effect of web buckling and shear on the overload capacity of an isolated stiffened panel under ice loading.

When ice-structure interactions are considered, proper modelling of the ice material is essential. Currently, a mature ice material model to capture the complicated mechanical behaviour of ice is still lacking. A few material models are available in the literature for the constitutive modelling of ice. Gagnon [7] modelled ice as a crushable foam plasticity material with volumetric hardening. Overlapping mesh layers were adopted to mimic high pressure and low pressure zones during ice crushing. Ice spalling was simulated by a predefined death time of contact between layers. The model was applied by Gagnon and Wang [8] in numerical simulations of a ship-ice collision to estimate the damage to a vessel. An alternative is to model ice using an elastic-plastic material model with the yield stress dependent on the hydrostatic pressure. Examples are Fish [9]; Derradji-Aouat [10]; Liu et al. [11] and Xu et al. [12]. In addition, Ince et al. [13] proposed a constitutive equation for ice materials, which associates the failure stress with the effects of strain rate, salinity and temperature. Both ductile and brittle behaviours are considered according to the level of strain rate. Fracture of ice was modelled using a cohesive zone model to define the crack-opening displacement. The ice model was employed in Ince et al. [14] to reproduce a drop test of ice on a deformable plate. Cai et al. [15] proposed to model ice material based on a soil and concrete constitutive material model with modified ice material properties applied. The model was used to simulate an ice impact experiment and showed good correlation. Han et al. [16] investigated several constitutive ice models and applied them to reproduce an ice crushing test.

For a better understanding of potential risks and consequences of accidental ice actions on offshore platforms in the Arctic, the Norwegian Petroleum Safety Authority (Petroleumstilsynet) initiated a series of projects to evaluate the structural safety of an offshore semi-submersible platform in the Northern areas of Norway [17–19]. This two-part companion paper discusses the findings for one of the most recent projects [17] carried out by ArcISo AS [20]. The studied site is the northernmost Block A in the 23rd licensing round (located at N74°, E35.67°). For the ice condition at the selected site, bergy bits and growlers (i.e., glacial ice features with a waterline diameter less than 15 m) are a major concern because they are relatively difficult to detect and monitor by current ice surveillance systems and are more difficult to handle by ice management operations, especially in extreme sea states. Paper I [21] describes a probabilistic analysis of ice impact velocities and impact locations under wave actions at different sea states. This Paper II presents investigations of the structural deformation, ice crushing, and ice-structure interactions using three different approaches, i.e., the integrated approach, weakly coupled approach and fully coupled approach. The critical local sharpness of ice is identified, i.e., the ice shape that produces the most severe structural damage for a given total energy dissipation. The results using different approaches are compared and discussed.

2. Impact energy from probabilistic analysis in paper I

A probabilistic analysis was conducted in Paper I [21], where a cuboidal glacial ice feature with dimensions of 15 m × 10.3 m × 10.3 m was driven by waves at different sea states and collided with the platform. The results showed that the impact velocities and impact heights are correlated. Assuming an encounter frequency of 10^{-3} per year, for a sea state with a return period of 1 year (a significant wave height of $H_s = 9.8$ m and a wave period of $T_p = 14.8$ s), the resulting ice impact velocity was calculated to be 3.81 m/s for a non-exceedance level of 90%. This velocity yields an impact energy of approximately 12 MJ for cuboidal ice and 6.5 MJ for
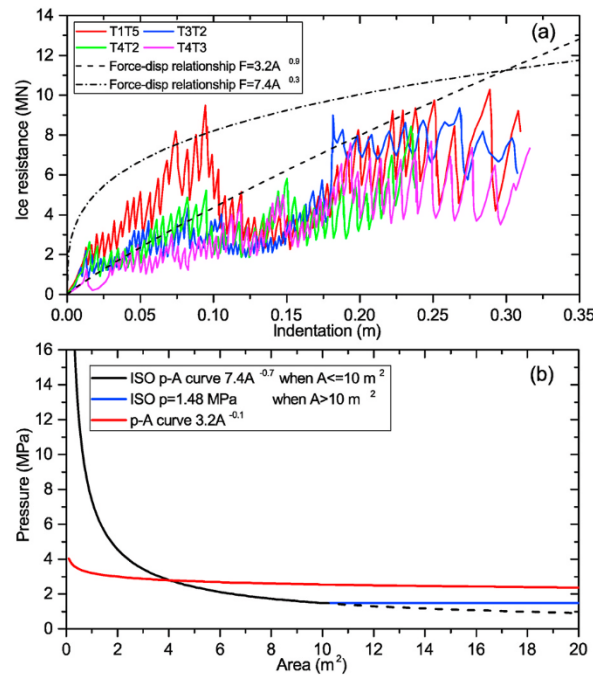
Fig. 3. (a) Force-displacement curves of the Pond Inlet tests [22] and (b) Pressure area relationships for the design ice from ISO 19906 standard and IACS PC3.

ellipsoidal ice with the dimensions $2a = 15$ m and $2b = 2c = 10.4$ m, where a, b and c represent the lengths of the three axes of the ellipsoid.

In addition, Lu et al. [17] investigated the capability of radar detection at different sea states and detection distances and discovered that the probability of detection for a 15-m-long glacial ice feature using conventional marine radar was less than 10% with a significant wave height of 5 m. The probability of detection increased to 50% for the features of 30-m-long glacial ice in the same wave condition. Considering the possibly increased ice dimension that may be undetected by a conventional maritime radar, the demand for total energy dissipation may increase. In this paper, for demonstration and conservative purposes, we adopt the kinetic energy levels of 7.5 MJ and 15 MJ for further damage assessments.

3. Ice pressure-area relationship for ALS conditions

A series of medium-scale indentation tests of ice that were conducted in 1984 were employed to calibrate the ice material model. The tests [22] were conducted using a spherical indenter with a radius of 2.3 m driven by 4 hydraulic actuators; each hydraulic actuator had a capacity of 4 MN. The indented ice face was located in a lateral tunnel excavated into the side of a grounded iceberg, near the settlement of Pond Inlet on the northern coast of Baffin Island [23]. Fig. 2 shows a sketch of the test arrangement.

Fig. 3 (a) shows plots of the force-displacement curves of 4 different cases from the Pond Inlet tests, with a common indenter radius of 2.3 m. The ice force indentation curves exhibit significant scatter, which demonstrates the inherent uncertainties of ice mechanical properties and responses. An analysis of the experimental data is carried out by averaging the ice energy absorption per unit crushed volume, which yields an ice crushing energy density of approximately 3 MJ/m^3 [18]. This ice energy density correlates well with a pressure area relationship of $p = 3.2A^{-0.1}$ (MPa), which is the local ice-load for Polar Class 3 (PC3) vessels in the IACS polar class code [24]. PC3 represents vessel capabilities in the year-round operation in second-year sea ice, which may include multiyear ice inclusions.

The ISO 19906 standard [1] recommends an ice pressure area relationship of $\begin{aligned} p &= 7.4A^{-0.7} \text{ (MPa)} \quad \text{when } A \leq 10 \, m^2 \\ p &= 1.48 \quad \text{(MPa)} \quad \text{when } A > 10 \, m^2 \end{aligned}$ for designing structures against local ice loading, mostly for the ULS design. A comparison of the IACS PC3 curve and the ISO curve for the ice pressure is given in Fig. 3 (b). The ISO curve gives a very large pressure for small nominal contact areas, but the pressure decreases rapidly when the nominal contact area increases. The local pressure is smaller than that for the ISO pressure-area curves for $A < 4 \, m^2$ and larger than that for $A > 4 \, m^2$. The ISO curve was derived from a series of indentation tests in the Beaufort Sea, including the Pond Inlet tests, and the values were determined by the mean value plus three times the standard deviation. This yields an approximate upper envelope of ice strength. The corresponding ice energy density is much larger than the average value from the tests, especially when the contact area is small; refer to Fig. 3 (a). In ALS conditions, large deformations are expected either in ice or the structure or both, and thus, require a more realistic representation of ice energy absorption. The IACS PC3 pressure-area relationship of $p = 3.2A^{-0.1}$ (MPa) fits the average ice energy absorption of the Pond Inlet experimental data, and therefore, is adopted for further analysis.
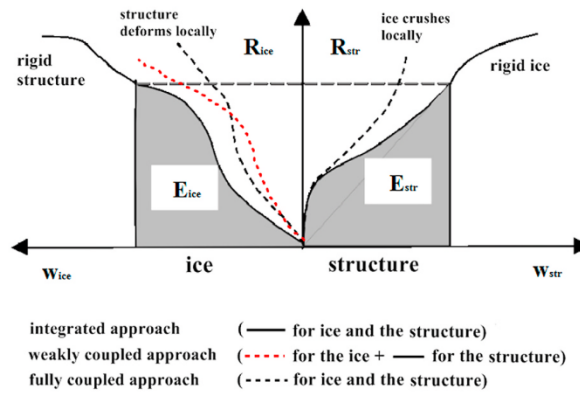
Fig. 4. A schematic sketch of the principles of damage prediction with three different approaches; picture modified from DNV-RP-C204 [25]. Note that the curves are only for illustration purposes and do not represent the true relative magnitude.
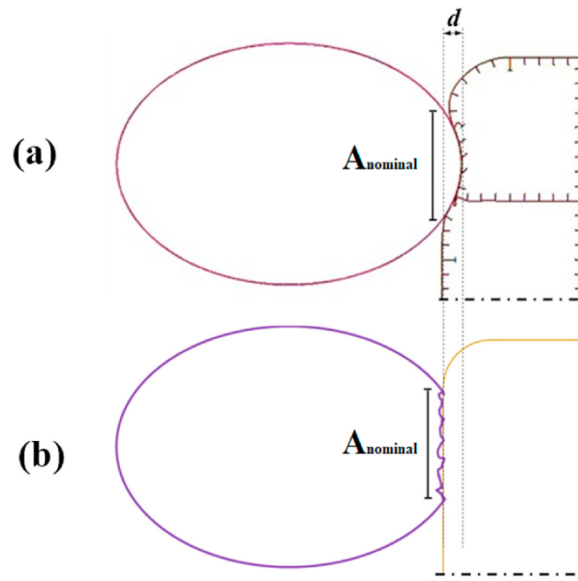

Fig. 5. The projected contact area (nominal area) as a function of (a) structure deformation and (b) ice crushing.

4. Methods for the analysis of ice impacts and ice-structure interactions

4.1. Integrated approach

The integrated approach originates from the method employed for ship collision analysis based on the shared energy methodology. The principle is sketched in Fig. 4 with solid lines. The force-deformation curve for the installation is established assuming that the ice is rigid. Likewise, the force-deformation curve for the ice is established assuming that the installation is rigid. For the same force level, both the ice and the installation shall deform and absorb energy. The resulting damage is determined when the energy dissipation, which is equal to the area under the force deformation curves, reaches the demand for total energy dissipation, as determined by the external mechanics analysis.

In this study, the resistance of the installation assuming rigid ice is obtained from nonlinear finite element simulations, while the ice resistance is in accordance with the selected force displacement curve of $F = 3.2A^{0.9}$ (MN), according to Section 3. In the integrated approach, the resistance of the ice or installation will not be influenced by each other during impact.

4.2. Weakly coupled approach

In contrast to the integrated approach, the weakly coupled method considers one-way coupling of the influence of structural deformation on the ice resistance curve. This is achieved by continuously comparing the ice resistance and structural capacity and

Table 1

Input parameters for the numerical simulations.

Parameter	Value	References
Ice density (kg/m^3)	900	ISO19906 [26]
Young's Modulus (GPa)	9.5	Timco and Weeks [27]
Poisson Ratio	0.3	Timco and Weeks [27]
Ice friction	0.15	Liu et al. [11]
Material coefficient a_0 (MPa^2)	2.588	Kierkegaard [28]
Material coefficient a_1 (MPa)	8.63	Kierkegaard [28]
Material coefficient a_2 (−)	−0.163	Kierkegaard [28]

updating their relative positions via iterations in the Simulator for Arctic Marine Structures (SAMS). SAMS (Lubbad et al., 2018) is a time domain solver for the simulation of marine structures under various ice conditions. The solver uses the discrete element method (DEM) that enables modelling the interactions between individual ice blocks (e.g., floe ice, level ice, ridges and icebergs) and the structure of interest. SAMS applies a novel implicit time stepping scheme and an improved contact model, enabling general visco-elastic contacts.

Similar to the integrated approach, the initial inputs of the weakly coupled method with SAMS are force-deformation curves for the installation assuming rigid ice and the ice curve based on the selected pressure-area relationship of ice or equivalent specific energy per unit crushed ice, but the difference is that SAMS continuously compares the ice resistance and structural capacity and updates their deformation and relative positions via iterations. The nominal area for the ice capacity should be calculated based on the ice displacement being the sum of ice crushing and structural deformation, refer to Fig. 5. Considering structural deformation, the ice capacity increases compared to that from the integrated method. More details on the weakly coupled method can be found in Lu et al. [17].

4.3. Fully coupled approach

The fully coupled approach considers mutual coupling between ice and the structure by constitutive modelling of the ice material in the nonlinear finite element analysis of structural response.

4.3.1. Ice material model

Ice as a material has complicated mechanical properties, which vary with location, temperature, grain size and orientation, as well as loading conditions (strain rate, confinement). Existing material models are still immature to comprehensively reproduce ice behaviours. To facilitate practical design of structures against abnormal ice loading, Liu et al. [11] developed an elastic-plastic isotropic material model for ice, where the material yield stress is dependent on the hydrostatic pressure to represent ice confinement. The model captures major characteristics of ice crushing and is adopted in the fully coupled approach together with the Bressan-Williams-Hill (BWH) fracture criterion (refer to Section 5.2) for modelling fracture of steel, such that the impact response of the ice, structure and their mutual interactions can be calculated simultaneously.

In the approach adopted by Liu et al. [11]; the behaviour of ice is modelled using the 'Tsai-Wu' elliptic yield criterion and a strain-based failure criterion that is dependent on the hydrostatic pressure. The yield surface as a function of both the second invariant of the deviatoric stress J_2 and the hydrostatic pressure p is defined as

$$J_2 = \frac{1}{2}S_{ij} : S_{ij} \tag{1}$$

$$f(p, \ J_2) = J_2 - \left(a_0 + a_1 p + a_2 p^2\right) = 0 \tag{2}$$

where a_1, a_2 and a_3 are material coefficients to be specified by users, and S_{ij} is the deviatoric stress tensor.

To simulate ice failure, an empirical failure criterion is adopted based on the effective plastic strain ε_{eq}^p and the hydrostatic pressure $p = -\frac{\sigma_{kk}}{3}$ (pressure positive in compression):

$$\varepsilon_f = \varepsilon_0 + \left(\frac{p}{p_2} - \gamma\right)^2 \tag{3}$$

where p_2 is the larger root of the yield function, and ε_0 and γ are the parameters to be calibrated to experiments.

The ice material properties employed in the simulation are given in Table 1. The material coefficients a_0, a_1 and a_2 correspond to an ice uniaxial compressive strength of 9.0 MPa and an ice uniaxial tensile strength of 0.82 MPa. The implementation has been verified in a single element test, where nodes on one end of the solid element is fixed against all degrees of freedom and nodes on the opposite plane are forced to move in a displacement-controlled manner. The resulting evolution of the yield stress with the hydrostatic pressure agrees with the theoretical curve, which demonstrates a sound implementation of the ice model.

It should be noted that we assume a low speed glacial ice impact process and therefore the strain rate is not considered for the selected constitutive ice model and no sensitivity analysis on strain rate effects is conducted. From probabilistic analysis in Paper I [21], the resulting ice impact velocity driven by waves and currents was calculated to be 3.81 m/s for ALS conditions with an
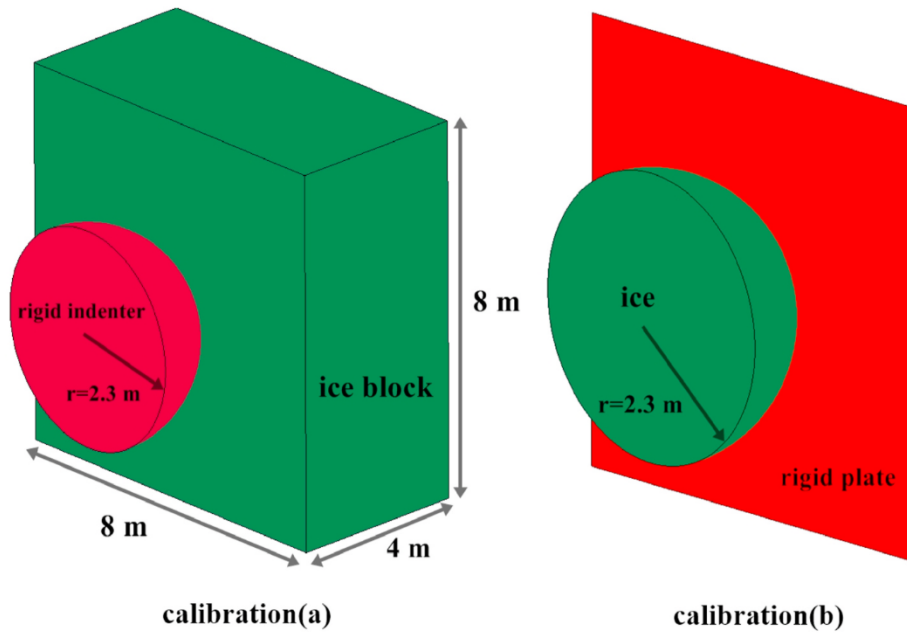
Fig. 6. Two methods for the calibration of the ice material: (a) rigid spherical indenter versus an ice block, yielding high ice confinement; (b) rigid plate versus a spherical ice, yielding low ice confinement.
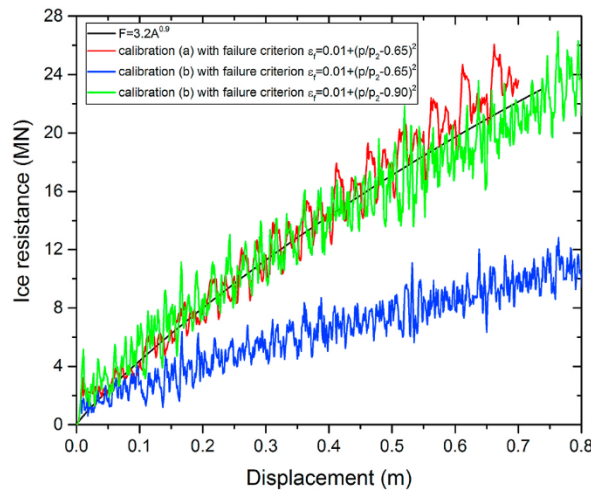

Fig. 7. Two different calibrations of the ice failure criteria for the design ice curve.

exceedance probability of 10^{-4} with respect to the design impact energy. This justifies the low speed impact assumption in glacial ice collisions.

4.3.2. Calibration of the ice model

The ice pressure-area relationship of $p = 3.2A^{-0.1}$ (MPa) for IACS PC3 vessels is employed in ALS analysis. Instead of calibrating directly to the pressure-area relationship, we calibrate to the force-displacement curve of $F = 3.2A^{0.9}$ (MN). Theoretically, both relationships should be similar. However, when the pressure-area relationship is applied, the pressure differences between the target and the simulation curves will be substantially reduced for large contact area conditions and may be easily overlooked. In addition, how the pressure-area relationship can be utilized directly to assess the structural deformation remains ambiguous.

Two ways exist to calibrate to the force-displacement relationship:

a) push a rigid indenter into a deformable ice block, as shown in the Pond Inlet tests and Fig. 6 (a)
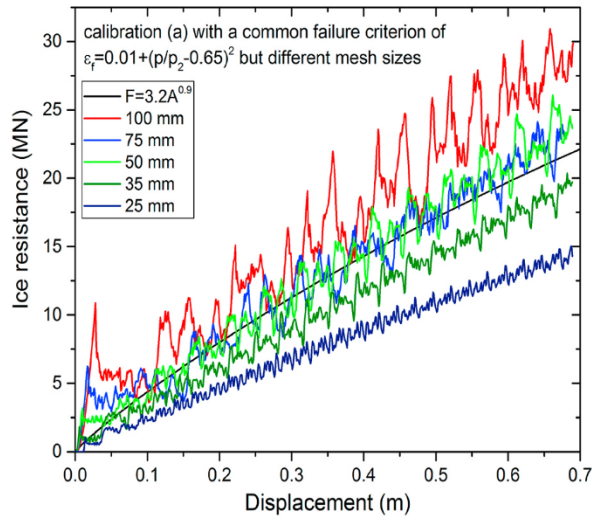b) use a rigid plate to crush a deformable spherical ice, as shown in Fig. 6 (b).

Fig. 8. Mesh size sensitivity of the ice model for the given ice shape.
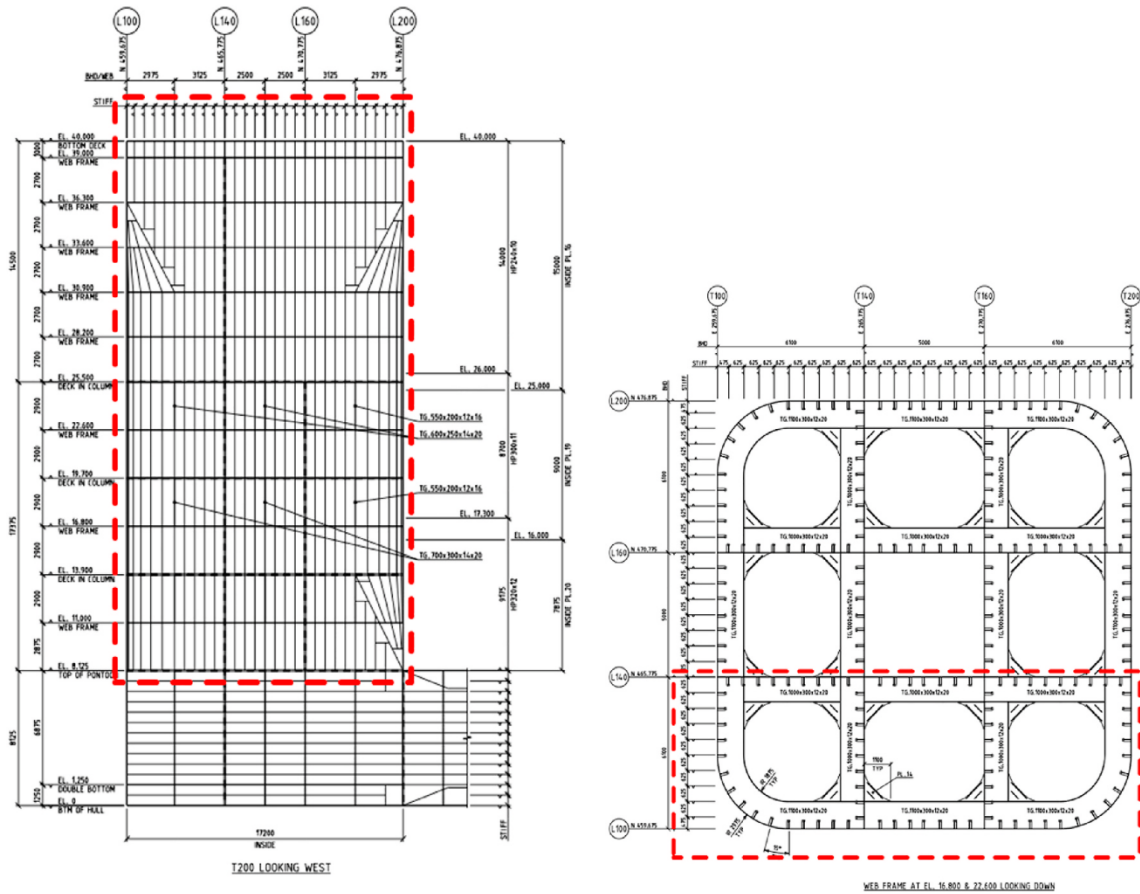

Fig. 9. Section of the column.

One may consider that the two calibrations can be applied interchangeably. However, the simulations contradict this notion. Fig. 7 shows the calibrated curves and ice failure criteria for the same design ice resistance curve using the two calibrations. A mesh size of 50 mm is adopted for the ice block in calibration type (a). For calibration type (b), meshing the spherical ice is difficult with a uniform mesh size; however, the mesh size is kept in the range of 35–75 mm. The results indicate that the two calibrations yield quite different
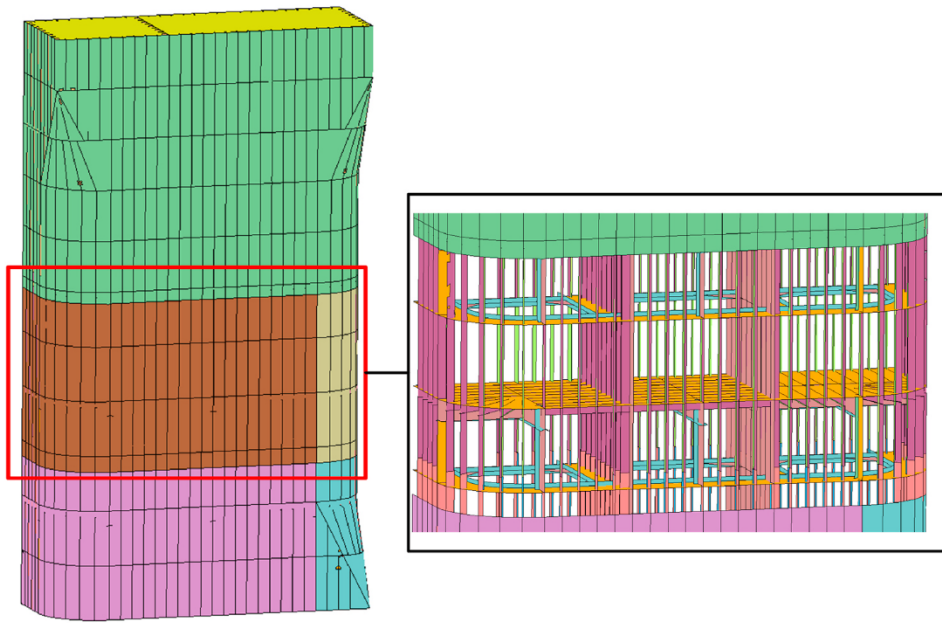
Fig. 10. Finite element model of the structure column.

Table 2
Properties of the steel material.

Steel Grade	Young's Modulus (MPa)	Yield Strength (MPa)	Poisson Ratio	Power law K (MPa)	Power law n
column plates	2.07×10^5	420	0.3	860	0.16
column HPs	2.07×10^5	355	0.3	780	0.22

long axis 2a=15 m
short axis 2b=2c=10.4 m
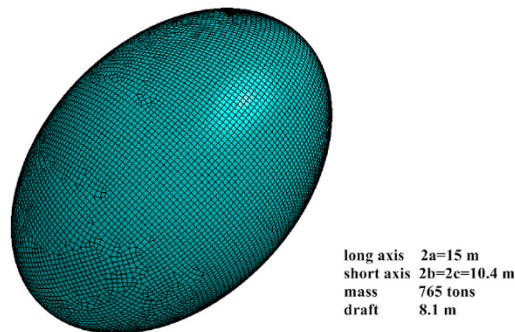mass 765 tons
draft 8.1 m

Fig. 11. Base case of ellipsoidal ice with 2a = 15 m

ice failure criteria. If the ice fracture criterion based on calibration (a) is used to simulate the (b) case, a much lower force level is obtained, which is less than half of the desired ice resistance.

The significant differences are mainly due to different ice confinements in the two calibrations: Calibration (a), in which a rigid spherical indenter crushes a deformable ice block, yields a more compact ice due to the confinement created by neighbouring ice, whereas the ice in calibration (b) is less confined. The ice confinement of the real collision events with deformable ice and structures is in between these two extremes. Therefore, given the same parameters for ice material and failure, the force levels are in the sequence of $F_{calibration(a)} > F_{ice-platform} > F_{calibration(b)}$, where $F_{ice-platform}$ is the contact force in a real collision event with deformable ice and structures. Therefore, if the ice failure criterion is calibrated to calibration (a), then we obtain $F_{calibration(a)} = 3.2A^{0.9} > F_{ice-platform}$. Conversely, $F_{ice-platform} > F_{calibration(b)} = 3.2A^{0.9}$ when calibrated to calibration (b). No direct evidence from tests is available to confirm the differences between the two calibrations. Initial analyses show that the use of calibration (a) would cause crushing of ice only and virtually no deformation of the structure. Due to the lack of more experimental evidence, calibration (b), which yield a stronger ice for ice-structure interaction analysis, was selected. This approach is considered conservative.
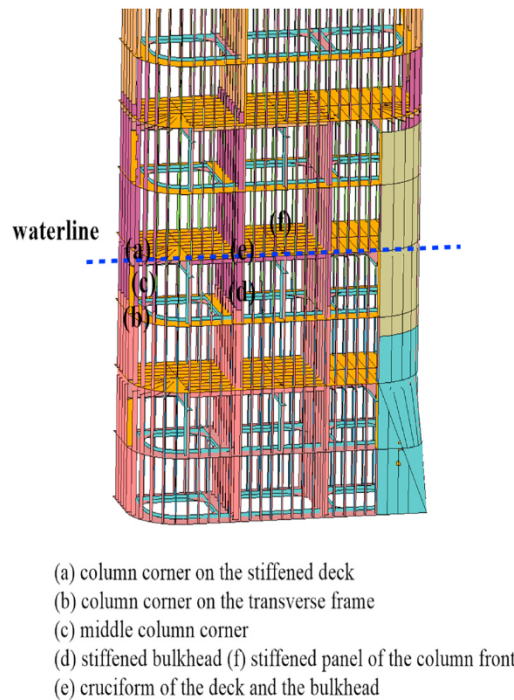
waterline

(a) column corner on the stiffened deck
(b) column corner on the transverse frame
(c) middle column corner
(d) stiffened bulkhead (f) stiffened panel of the column front
(e) cruciform of the deck and the bulkhead

Fig. 12. Impact locations on the platform column for which the structure force-deformation curves have been determined using FEM simulations.
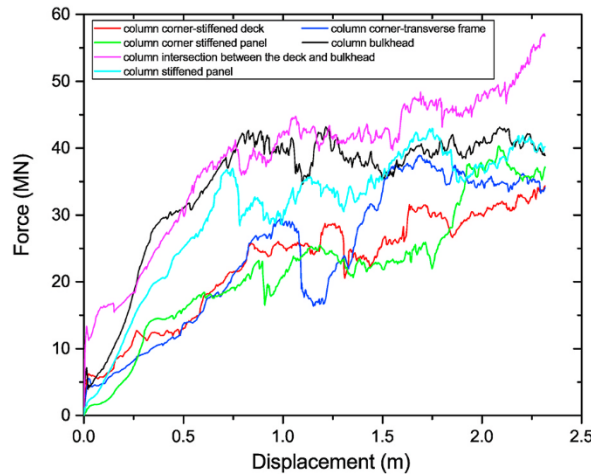

Fig. 13. F-D curves of the platform column at the 6 simulated impact locations. The rigid ice is ellipsoidal with 2a = 15 m and 2b = 2c = 10.4 m

A study of the mesh size sensitivity of the ice model is conducted using calibration (a), where the mesh size of the ice block can be well controlled. Fig. 8 shows the simulation results with five different mesh sizes 100 mm, 75 mm, 50 mm, 35 mm and 25 mm for the ice block and a common ice failure strain of $\varepsilon_f = 0.01 + (p/p_2 - 0.65)^2$. The results indicate that the ice material model with a strain-based fracture criterion is very sensitive to the adopted mesh size. This can be expected because models with finer meshes are more likely to capture highly concentrated local strains, while coarser meshes will blur local strain details by averaging the stress and strain within an element. Therefore, for the same failure strain criterion of ice, models with a finer mesh will be eroded more easily compared with those with a coarser mesh, and thus, give a lower force level. This is analogous to the mesh size sensitivity of fracture prediction of steel plates modelled with large shell elements.

One solution to this sensitivity is to use the same mesh size as employed in the calibration. It is however difficult to mesh the target ellipsoidal or spherical ice shape with uniform sizes. A viable approach for the calibration of the ice model, accounting for the mesh size sensitivity, is to calibrate the design ice curve on a case-by-case basis instead of relying on a single calibration and applying the calibrated fracture criterion for all shapes. In this approach, each ice shape and meshing will require a new calibration for the ice
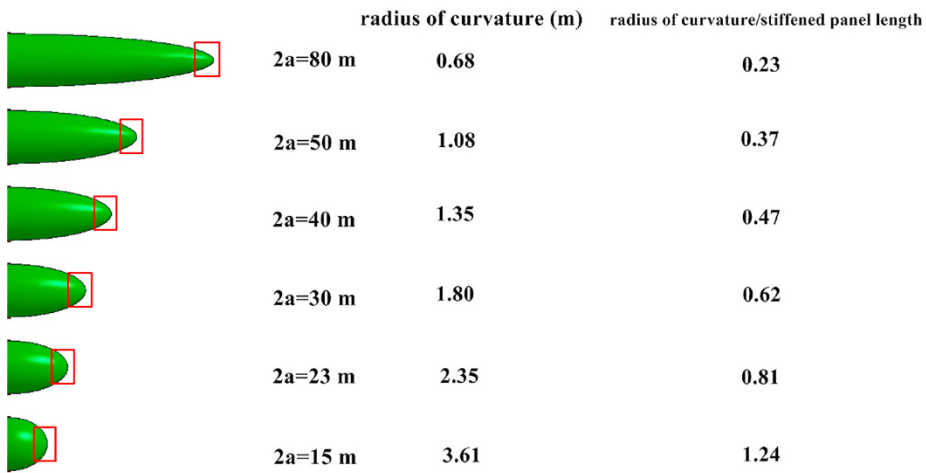
	radius of curvature (m)	radius of curvature/stiffened panel length
2a=80 m	0.68	0.23
2a=50 m	1.08	0.37
2a=40 m	1.35	0.47
2a=30 m	1.80	0.62
2a=23 m	2.35	0.81
2a=15 m	3.61	1.24

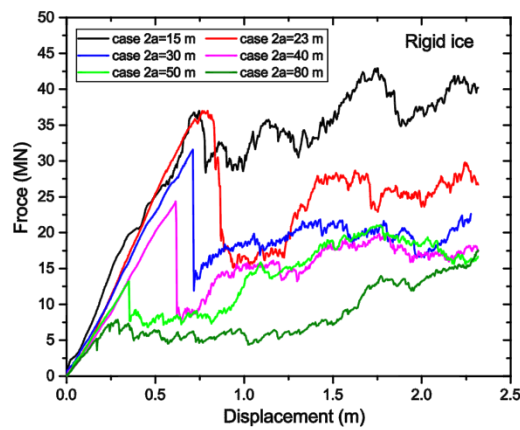**Fig. 14.** Ellipsoidal ice models with different sharpness.

Fig. 15. Force displacement curves of stiffened panels in the platform column subjected to impacts from rigid ice with a common short axis of 5.2 m and different long axis.
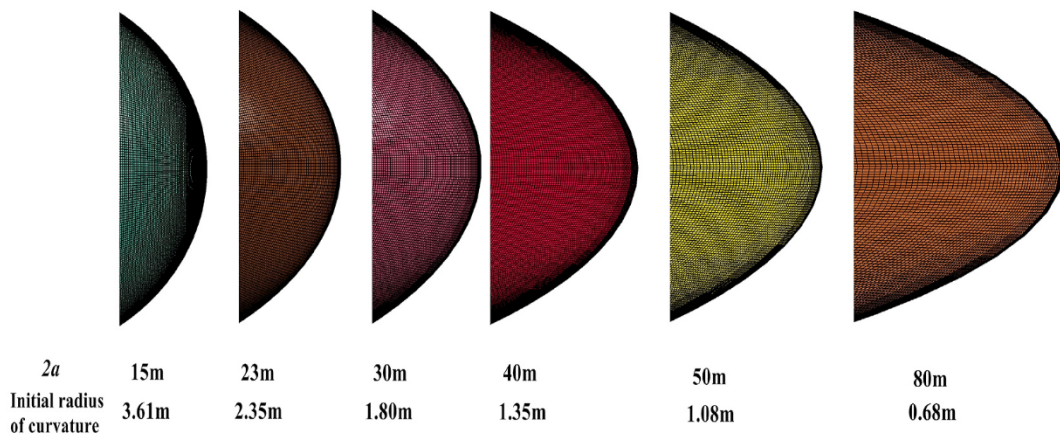
2a	15m	23m	30m	40m	50m	80m
Initial radius of curvature	3.61m	2.35m	1.80m	1.35m	1.08m	0.68m

Fig. 16. Modelling of ellipsoidal ice with different local sharpness using solid elements.
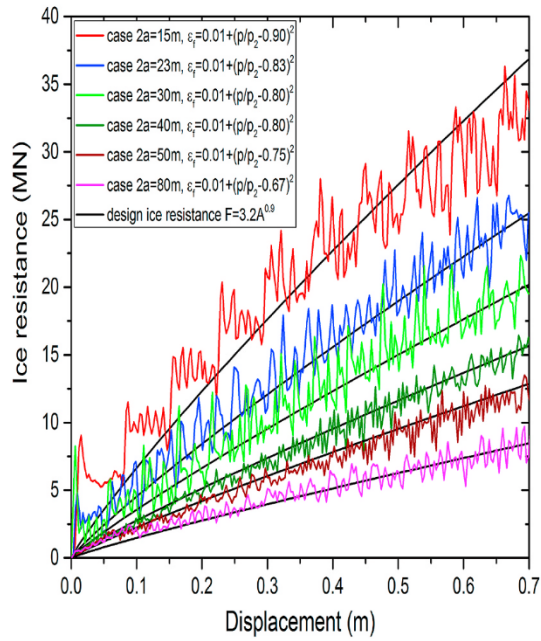
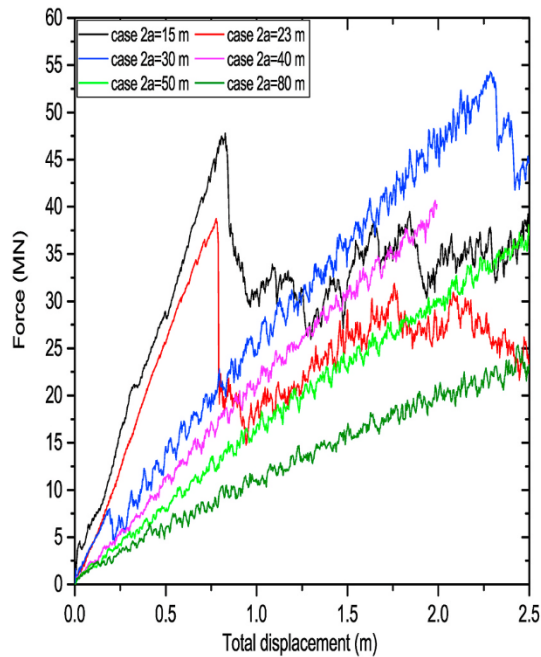**Fig. 17.** Case-by-case calibration of ellipsoidal ice with different sharpness.

Fig. 18. Force versus total displacement curves for column stiffened panels under impacts from different ellipsoidal ice geometries.

failure strain. This strategy is adopted in this paper, and the corresponding calibration parameters are given for each ice shape when present.

5. Finite element model of a semi-submersible platform column

5.1. Model of the semi-submersible column

A finite element model for the column leg of the Midgard platform was adopted for the ice impact analysis. The platform column
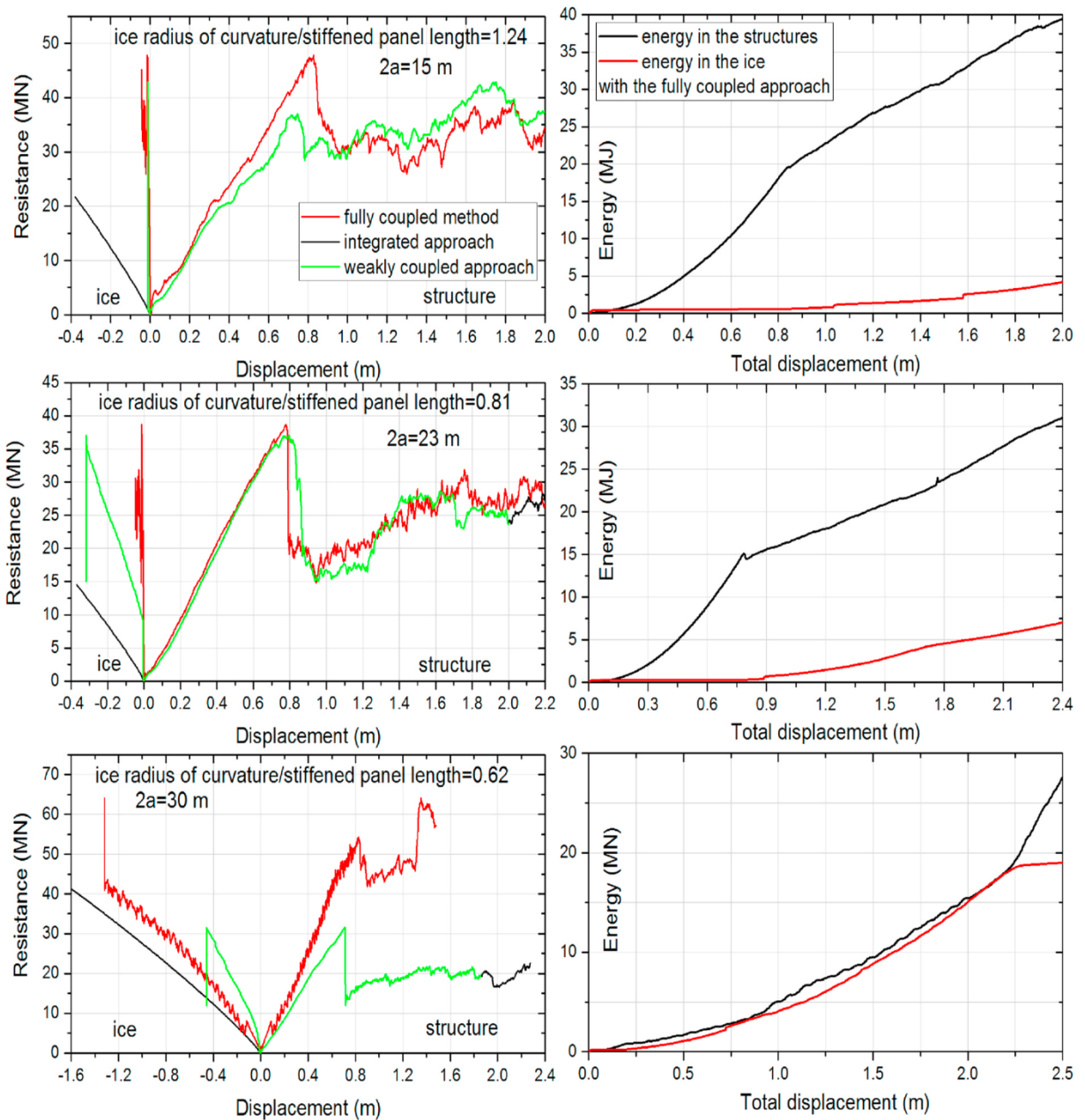
Fig. 19. Force-displacement and energy absorption curves of ice and structures using fully coupled simulations for the case of 2a = 15 m, 23 m, and 30 m.

was modelled by Tavakoli and Amdahl [29] for the assessment of structural strength against supply vessel collisions. Drawings of the platform column are shown in Fig. 9. The column was modelled from EL8125 to EL39000 in Fig. 9. Only the front part of one leg was modelled. The overall dimensions of the column finite element model are 17,200 mm × 30,875 mm × 6100 mm (w × h × d).

The finite element model of the column is shown in Fig. 10. The column outer shell thickness is in the range of 16–18 mm. Vertical stiffeners are equally spaced on the shell plating every 0.625 m. The stiffeners were modelled as L-bars with the dimensions of 320 × 50 × 12 × 40 (mm), 300 × 50 × 11 × 50 (mm) and 240 × 40 × 10 × 30 (mm) depending on the locations. The column decks and the vertical bulkheads are equipped with stiffeners every 0.625 m. The thickness of the deck shell plating is 12 mm, and that of the bulkhead plating is 14 mm. The column model was meshed using approximately 245,000 shell elements. The general element size is 120 mm.
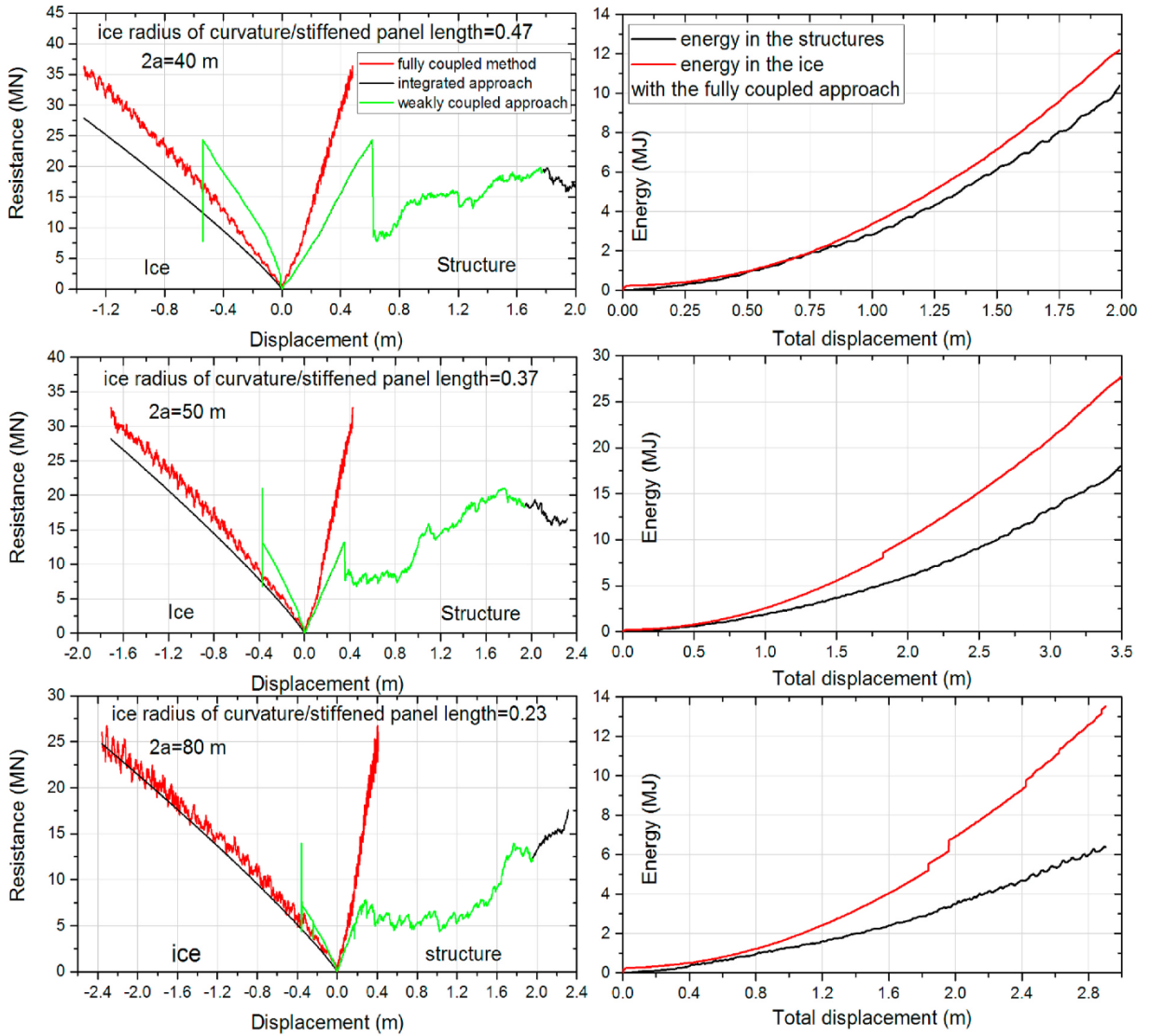
Fig. 20. Force-displacement and energy absorption curves of ice and the structures using fully coupled simulations for the case of 2a = 40 m, 50 m, and 80 m.

5.2. Material and fracture modelling

When ice-structure interactions are considered, proper modelling of the material behaviour is essential because the relative strength of the striking ice and structure is very sensitive to the material strength and fracture. A rupture of structures can easily shift their strong sides.

Power law hardening with a yield plateau is employed to model the material. The hardening is described by the yield criterion

$$f = \sigma_{eq} - \sigma_f\left(\varepsilon_{eq}\right) = 0 \tag{4}$$

where σ_{eq} is the von-Mises equivalent stress. The current flow stress σ_f is a function of the equivalent plastic strain ε_{eq} via the power law hardening rule:

$$\sigma_f\left(\varepsilon_{eq}\right) = \begin{cases} \sigma_0 & if \ \varepsilon_{eq} \leq \varepsilon_{plateau} \\ K\left(\varepsilon_{0,eff} + \varepsilon_{eq}\right)^n & if \ \varepsilon_{eq} > \varepsilon_{plateau} \end{cases} \tag{5}$$

where K and n are the hardening parameters and σ_0 is the initial yield stress.

The BWH instability criterion is employed to model the fracture of steel in the ice collision simulation. The BWH instability criterion was proposed by Alsos et al. [30] and combines Hill's local necking model [31] and the Bressan-Williams shear stress criterion
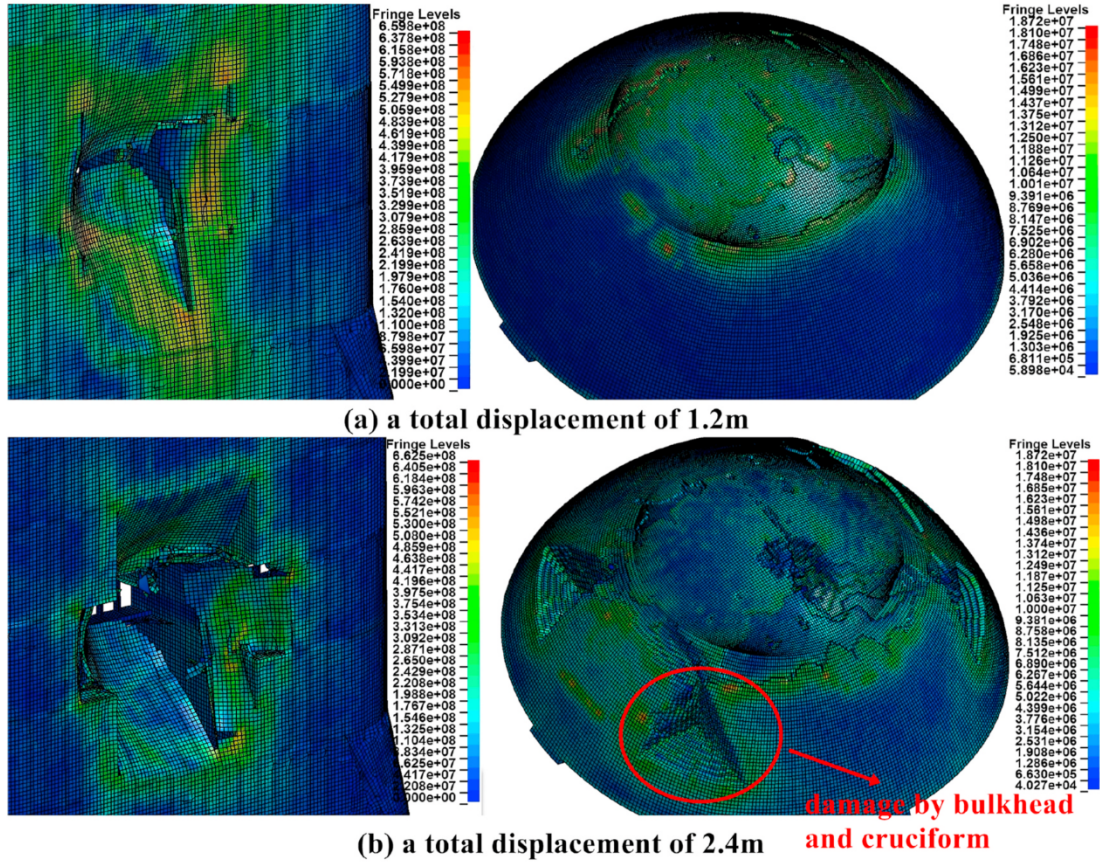
Fig. 21. Structural damage and ice crushing for the case of 2a = 15 m with the fully coupled approach.

[32]. The BWH criterion considers that fracture occurs at the onset of the local necking instability and disregards the post-necking regime, which is conservative. The excellent accuracy of the BWH criterion has been validated of good accuracy by comparison with various collision experiments [33,34]. The BWH criterion can be expressed in the principle stress space as

$$\sigma_1 = \begin{cases} \dfrac{2K}{\sqrt{3}} \dfrac{1+\frac{1}{2}\beta}{\sqrt{\beta^2+\beta+1}} \left(\dfrac{2}{\sqrt{3}} \dfrac{\widehat{\varepsilon}_1}{1+\beta} \sqrt{\beta^2+\beta+1} \right)^n & if \;\; -1 < \beta \le 0 \\[4mm] \dfrac{2K}{\sqrt{3}} \dfrac{\left(\frac{2}{\sqrt{3}} \widehat{\varepsilon}_1 \right)^n}{\sqrt{1 - \left(\frac{\beta}{2+\beta} \right)^2}} & if \;\; 0 < \beta \le 1 \end{cases} \tag{6}$$

where β is the ratio of the minor principal strain rate to the major principal strain rate, $\beta = \dot{\varepsilon}_2/\dot{\varepsilon}_1$. The critical strain $\widehat{\varepsilon}_1$ can be assumed to be equal to the power law coefficient n in accordance with Hill's criterion.

Fracture is simulated by eroding elements when the fracture criterion is fulfilled. A through-thickness integration point is failed by setting the stresses to zero once the failure criterion is satisfied. Element erosion occurs once the middle integration point fails.

Two kinds of steel material grades are employed for the structures; the material properties are shown in Table 2. The column plates are equipped with a yield stress of 420 MPa, while the column stiffeners are fabricated with a steel yield stress of 355 MPa.

5.3. Resistance of the platform column to rigid ice impacts

Both the integrated approach and the weakly coupled approach require force-displacement curves of structures impacted by rigid ice as inputs prior to further analysis. This section investigates the structural capacities of the column by pushing rigid ice into the structures. The considered glacial ice is confined to bergy bits due to the limited capability of the radar detection, which ranges from 5 m to 15 m in the projected waterline length. Therefore, the base case of the rigid ice is ellipsoidal with a long axis of 2a = 15 m and a short axis of 2b = 2c = 10.4 m, as shown in Fig. 11. This geometry is consistent with the ice geometry employed in related previous studies [35] and ST19 [18]. The long axis of the base ice geometry will be varied in subsequent sections to study the influence of local
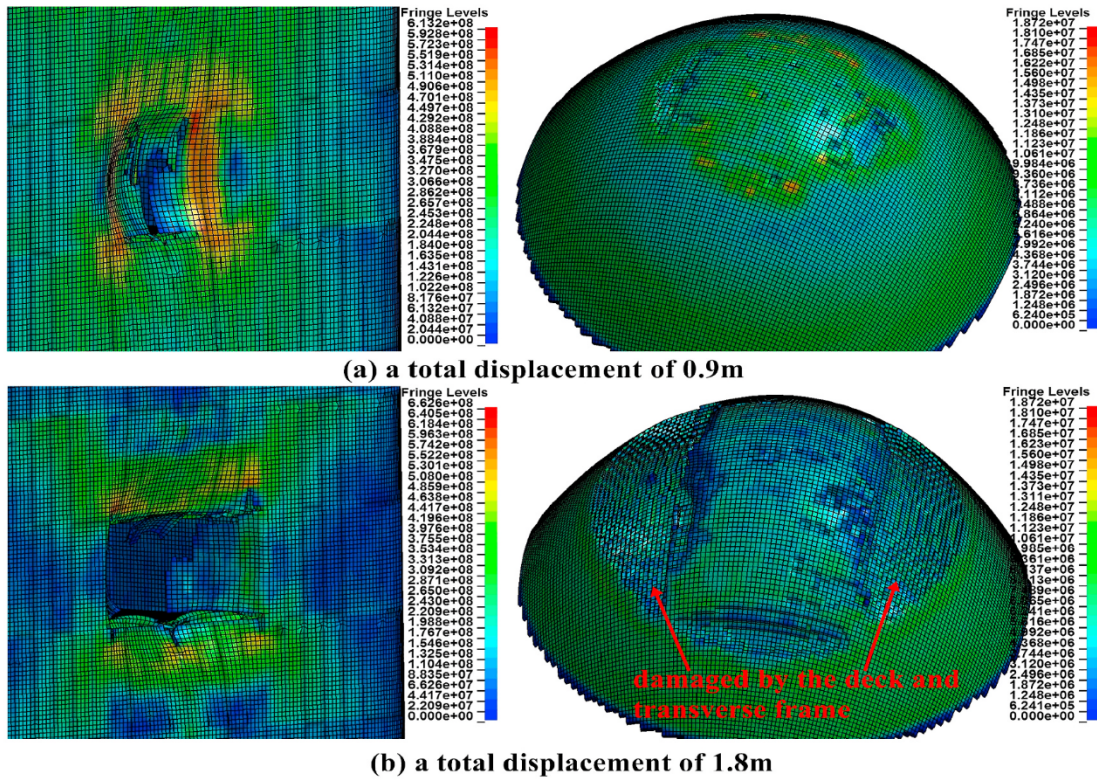
(a) a total displacement of 0.9m

damaged by the deck and
transverse frame

(b) a total displacement of 1.8m

Fig. 22. Structural damage and ice crushing for the case of 2a = 23 m with the fully coupled approach.

ice sharpness on the structural response.

The ice impact analysis is carried out using the explicit NLFEA software LS-DYNA 971. The four-node Belytschko-Lin-Tsay shell element with reduced integration was employed with 5 integration points through the thickness. Hourglass stiffness is added using the stiffness-based form (option 4 in LS-DYNA). This approach is very efficient and gives a low dissipation of spurious hourglass energy (less than 2–3%). The rear side, top and bottom of the column are constrained in all degrees of freedom. The rigid ice model is given a prescribed motion velocity of 3 m/s, and any strain rate effect is not taken into account. Two kinds of contacts are defined in this analysis, i.e., self-contact and master-slave contact. For the rigid ice-structure collision, the master-slave contact is employed with the structure as the slave part. Self-contacts are defined for the structure to detect possible internal contacts of structural members due to deformation. A static friction coefficient of 0.3 was employed for all contacts.

With the numerical settings and material model, the force displacement curves at different locations of the platform column impacted from the base ice geometry feature with 2a = 15 m can be obtained. The characteristic locations on the platform column are shown in Fig. 12, and the corresponding force-displacement (F-D) curves are plotted in Fig. 13. The column bulkhead and intersection between the bulkhead and the deck represent strong spots of the structure, while the column corner structures are relatively weak.

6. Identification of critical local sharpness of ice with respect to penetration of the column stiffened panels

During glacial ice impacts, the ice-structure interactions are challenging yet crucial for structural safety considerations. On the structure side, assuming a rigid ice feature, the sharper is the local ice geometry, the greater is the chance that the structure will rupture. Examples are illustrated in Fig. 14, where rigid elliptical ice models with a common short axis of 2b = 10.4 m but different long axes of 2a = 15 m, 23 m, 30 m, 40 m, 50 m and 80 m collide with stiffened panels of the platform column front. The length of the stiffened panels along the stiffener is 2.9 m, which yields the ratios of ice radius of curvature over the panel length of 1.24, 0.81, 0.62, 0.47, 0.37 and 0.23. The resulting force displacement curves are plotted in Fig. 15. The results confirm that a sharper ice local geometry induces more localized structural deformation and causes early fracture.

However, when realistic ice properties are considered, a sharp ice geometry will be crushed more easily than a blunt ice geometry. The ice crushing makes the glacial ice feature less sharp and increases the contact area. By considering both realistic ice properties and a deformable structure, it should be possible to identify an ice geometry such that the ice is sufficiently sharp to induce early steel fracture, and at the same time the ice is sufficiently blunt and strong to withstand the structural resistance before steel fracture. To find the critical local ice sharpness, the fully coupled approach is mainly adopted while the weakly coupled and integrated methods are employed for comparison. Before these analyses can be undertaken, case-by-case calibration of the ice model in the fully coupled approach is needed.
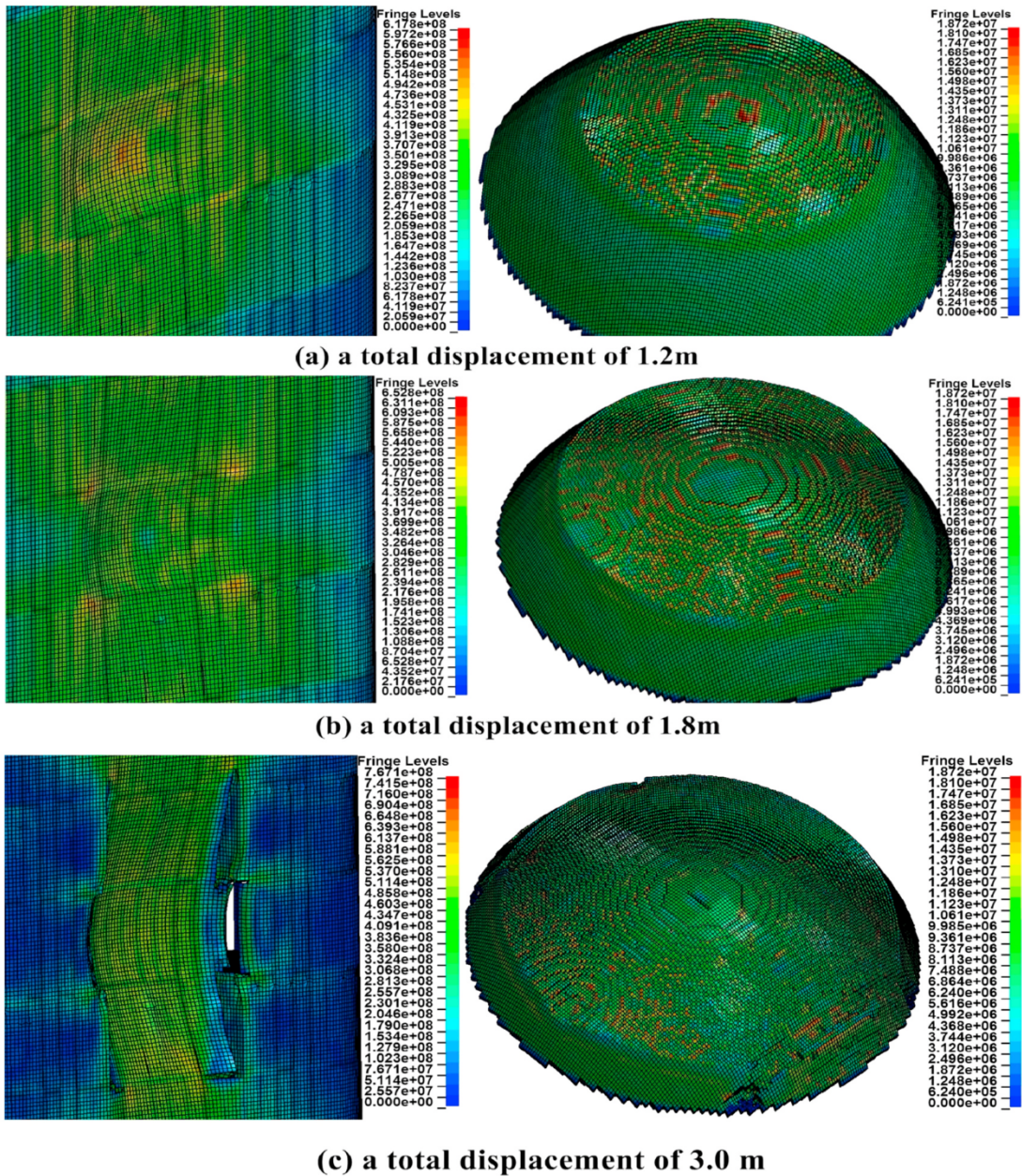
(a) a total displacement of 1.2m

(b) a total displacement of 1.8m

(c) a total displacement of 3.0 m

Fig. 23. Structural damage and ice crushing for the case of 2a = 30 m with the fully coupled approach.

6.1. Case-by-case calibration of the ice model

The ice model employs a strain-based fracture criterion for ice failure, which renders the model sensitive to the adopted mesh size, as discussed in Section 4.3.2. Furthermore, as modelling the target ellipsoidal shapes of ice with the same mesh size is difficult, calibration was performed on a case-by-case basis. Six ellipsoidal ice geometries with different levels of sharpness are shown in Fig. 16. The sizes of the ice solid elements generally range from 35 to 75 mm.

The 6 ellipsoidal ice models are calibrated to the target ice design curve of $F = 3.2A^{0.9}$ (MN) in Fig. 17 by crushing the ice model with rigid plates, i.e., calibration (b) in Fig. 6 (b). In the fully coupled simulations, the eroded_single_surface contact is applied to define the internal contact of the ice, and the eroded_surface_to_surface contact is applied to define the contact between ice and the structure using the pinball segment-based contact with SOFT = 2. An ice friction coefficient of 0.15 is employed. The results show that the largest force-deformation curve is obtained with the bluntest ice but the force versus area relationship is the same for all shapes. Generally, the calibrated force curves follow the design ice resistance curve well with small oscillations. The calibrated ice failure strain tends to
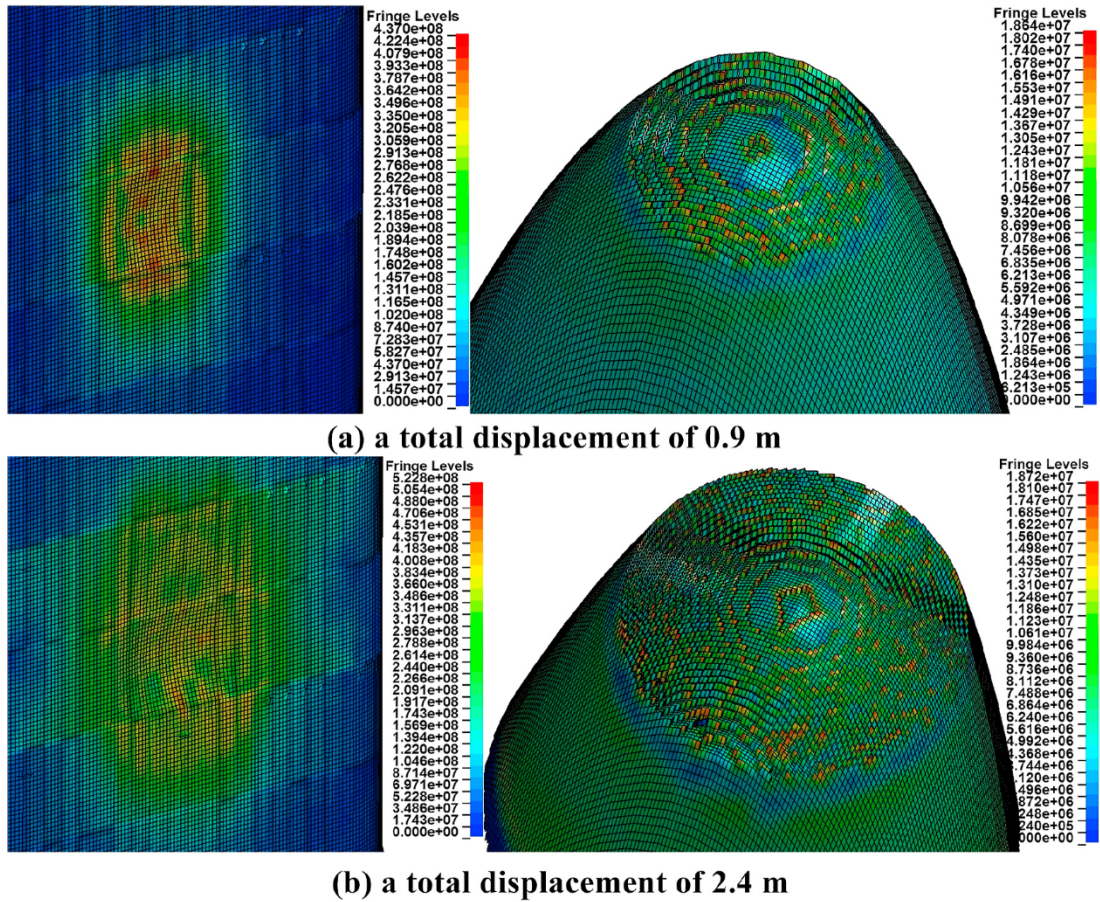
(a) a total displacement of 0.9 m

(b) a total displacement of 2.4 m

Fig. 24. Structural damage and ice crushing for the case of 2a = 80 m with the fully coupled approach.
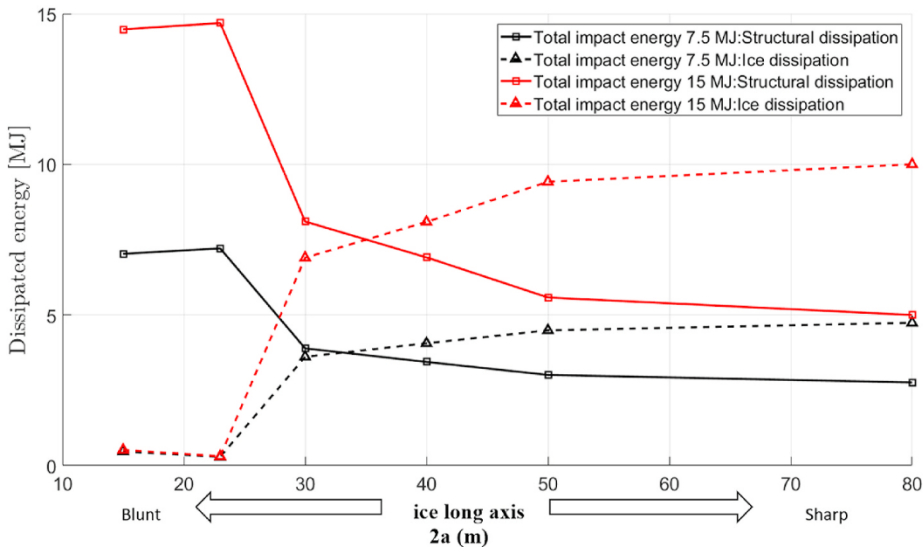

Fig. 25. Energy dissipation between the structure and ice with varying sharpness levels, as simulated by the fully coupled approach.
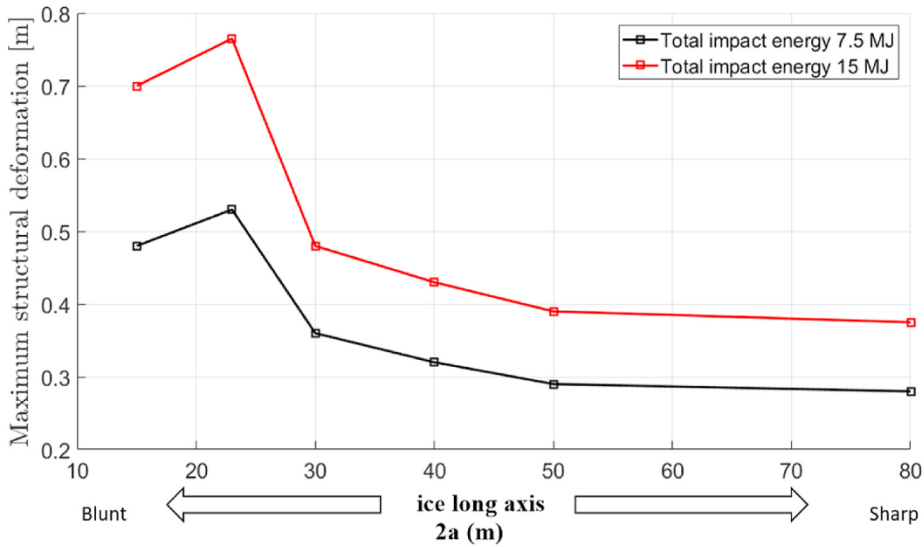
Fig. 26. Structural deformation under the impact of glacial ice features with different sharpness levels.
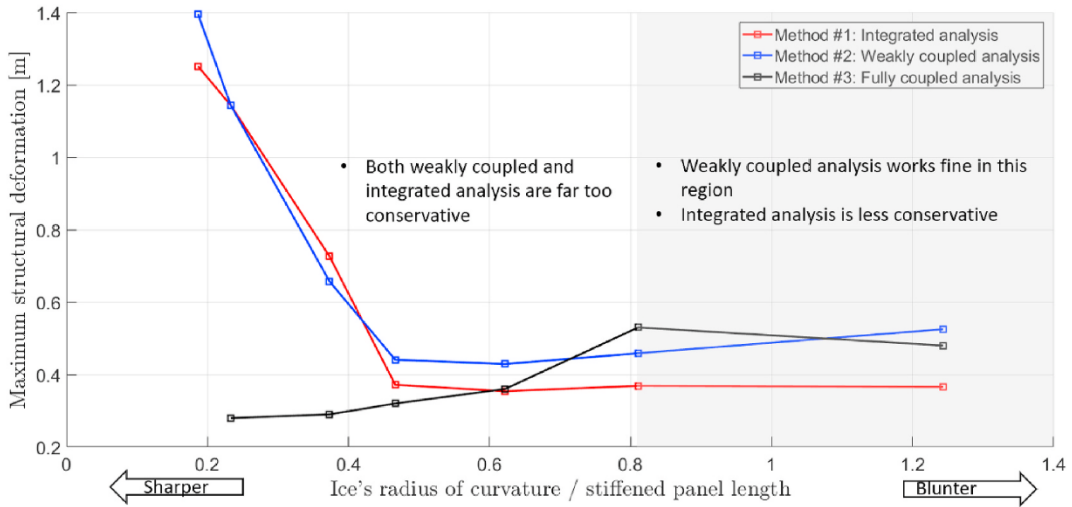

Fig. 27. Maximum structural deformation with a total energy dissipation of 7.5 MJ for all three different methods for various glacial ice feature sharpness (each marker of the same colour represents a glacial ice feature with its long axis 2a = 80, 50, 40, 30, 23, 15 m from left to right). (For interpretation of the references to colour in this figure legend, the reader is referred to the Web version of this article.)

decrease as the ice geometry becomes sharper. The ice models and associated calibrated ice failure criteria will be employed in subsequent simulations of ice-platform column impacts.

6.2. Identification of critical ice sharpness

The calibrated 6 ellipsoidal ice models are used to impact the stiffened panels in the platform front using the fully coupled approach. The resistance versus total displacement, i.e., the deformation of both ice and the structure, is plotted in Fig. 18. The ice resistance dominates ellipsoidal ice with 2a = 40 m, 50 m and 80 m, whereas the structural resistance dominates ellipsoidal ice with 2a = 15 m and 23 m. The resulting force versus deformation relationships between the ice and the structure and the corresponding energy dissipation are plotted in Figs. 19 and 20, respectively.

For a relatively blunt ice geometry with 2a = 15 m and 23 m, the ice undergoes little deformation, and most energy is dissipated by the structure. This represents the ductile design of the structure. When the long axis is increased to 2a = 30 m, the ice starts to be crushed significantly, and large structural deformation simultaneously occurs in the structure. In this case, almost half of the energy is absorbed by the ice and the other half is absorbed by the structure. By further increase in the long axis to 2a = 40 m, 50 m and 80 m, the
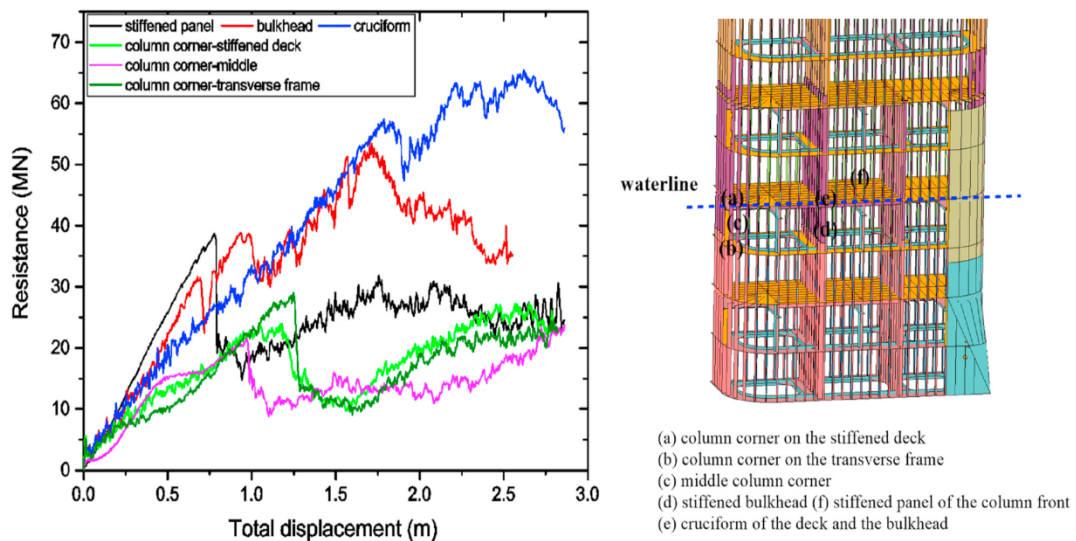
Fig. 28. Force versus total displacement curves for ice impacts on different locations of the platform column.

ice is crushed continuously and an increased proportion of the total energy is absorbed by the ice. However, the structure still dissipates considerable energy. This may be classified as shared energy design.

The resistance curves calculated from the integrated approach, weakly coupled approach and fully coupled approach are compared in Figs. 19 and 20. Significant ice-structure interaction is observed. When the long axis of the ellipsoidal ice is 2a = 15 m and 23 m, the ice is rather strong. The structural resistance agrees with that from the analysis with rigid ice. The force displacement curves from the fully coupled analysis and the weakly coupled approach are, however, significantly larger than the design ice resistance of $F = 3.2A^{0.9}$ (MN) due to an increase of the actual contact area and the update of relative positions of the ice and structure.

When the long axis is increased to 2a = 30 m, 40 m, 50 m and 80 m, both the ice and the structure deform and absorb energy. The force-deformation curves for the ice from the weakly coupled and fully coupled simulations appear larger than those of the integrated approach, while on the structure side, the fully coupled approach yields significantly larger resistance than that of the integrated approach. The differences in the results predicted by the three approaches come from different treatment of ice-structure interaction. Implicitly, the integrated approach and weakly coupled approach assume that the ice geometry does not change significantly during ice crushing such that the resulting F-D curve of the structure does not substantially deviate from that of the structural curve assuming rigid ice. Once extensive ice crushing occurs, the F-D curve of the structure increases due to an increase in the contact area. This effect can only be captured by the fully coupled approach, where mutual interactions of ice crushing and structural deformation are considered. The weakly coupled approach is superior to the integrated approach because it captures the one-way coupling by considering the influence of structural deformation on the ice resistance.

For the cases with 2a ≥ 30 m, the fully coupled method does not predict fracture of the outer shell at the displacement, where rupture occurs by assuming rigid ice. This is due to the increased actual contact area caused by deformation of both the ice and the structure and update of their relative positions, which relieves the local stress and strain concentrations. Hence, for analysing the impacts from sharp ice, the integrated approach and weakly coupled approach may yield overly conservative predictions for the structure. The two approaches are more suitable for cases with blunt ice, where ice crushing is minor and its influence on the structural resistance is negligible.

The structural damage and ice crushing from the fully coupled simulation at different characteristic displacements are visualized in Figs. 21 and 22 for the blunt ice with 2a = 15 m and 23 m, and Figs. 23 and 24 for the sharp ice with a long axis of 2a = 30 m and 80 m.

As shown in Fig. 21 with 2a = 15 m, the ice penetrates the column stiffened panel with minor ice damage. As the displacement increases, extensive damage to the platform deck and bulkhead also occurs, whereas the intersection of the deck and bulkhead or a frame represents "hard spots" of the structure, which is capable of substantially crushing the ice. In the case of 2a = 23 m (refer to Fig. 22), the ice is capable of penetrating the outer shell with minor ice crushing. The total energy dissipation accumulates to 15 MJ at the onset of rupture in the shell plating. When the contact spreads to the transverse frame or deck, the ice starts to undergo significant crushing.

When the long axis changes from 2a = 23 m to 2a = 30 m in Fig. 23, there is a drastic transition from ductile behaviour with minor ice damage to shared energy behaviour with significant ice crushing. During this process, the structure is deformed severely, and fracture occurs along the bulkhead at a very late stage for a total displacement of 3.0 m. The fracture pattern is different from the rupture of the stiffened panels in the case 2a = 15 and 23 m. Similar ice crushing and structural deformation are observed for cases with increased long axes but rupture of the structure does not occur for the considered impact energy.

Assume that the total impact energy that should be dissipated by the ice and structure is 7.5 MJ or 15 MJ according to the findings from Paper I. Fig. 25 shows the portion of the impact energy that will be dissipated by crushing the ice and deforming the structure for
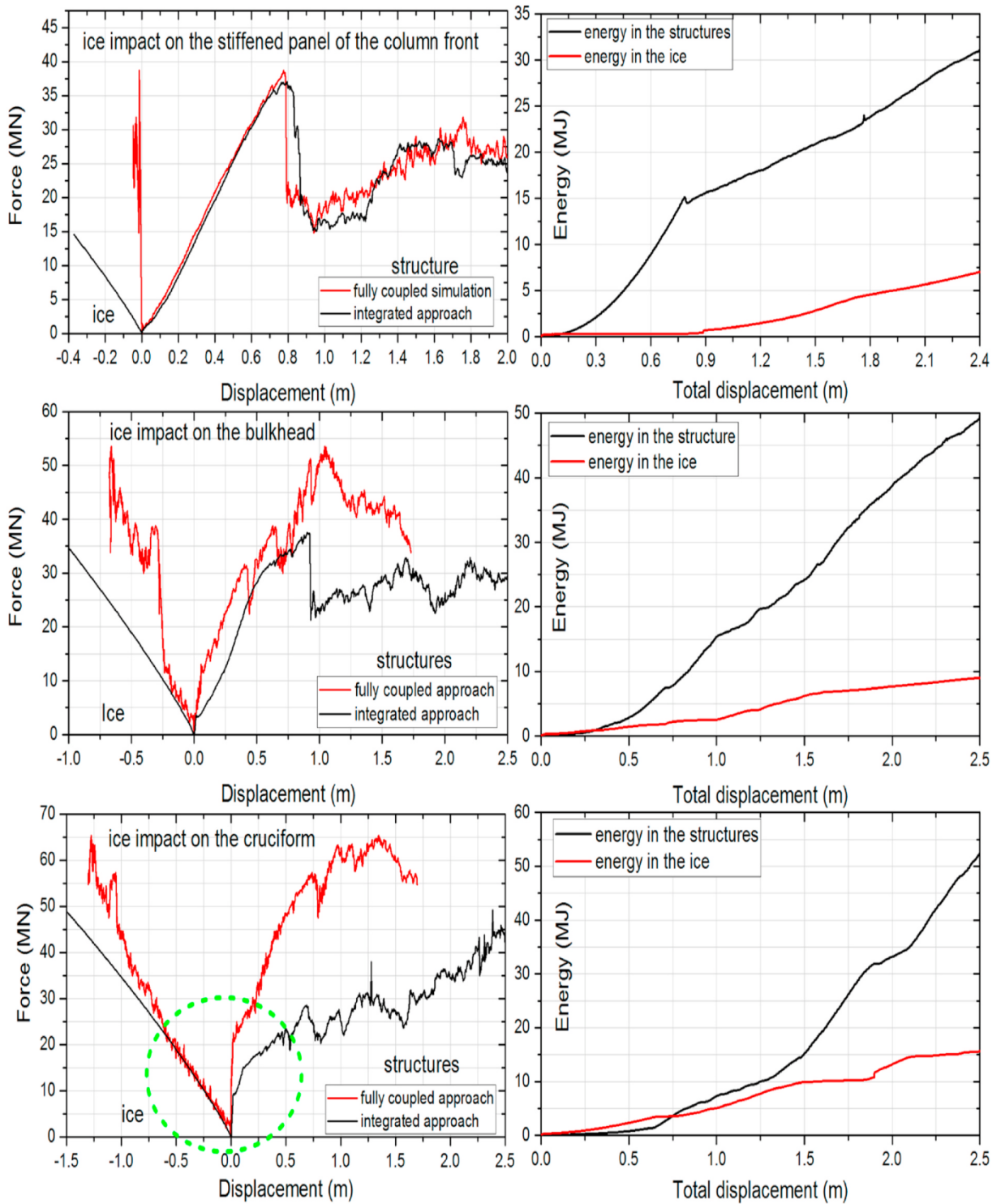
Fig. 29. (Left) Structural damage and ice crushing for ellipsoidal ice with 2a = 23 m that impacts the stiffened panel, bulkhead and intersection between a deck and bulkhead of the platform column. Integrated approach means that either ice or structure is rigid. (Right) Energy dissipation in structure and ice from fully coupled analysis.

various levels of local ice sharpness. The corresponding maximum structural deformation is plotted in Fig. 26. For the cases with blunt ice, most of the total energy is dissipated by structural deformation, while for the cases with sharp ice, the ice will be crushed significantly, and the structure simultaneously dissipates considerable energy. Between the two extremes, a sudden transition from the
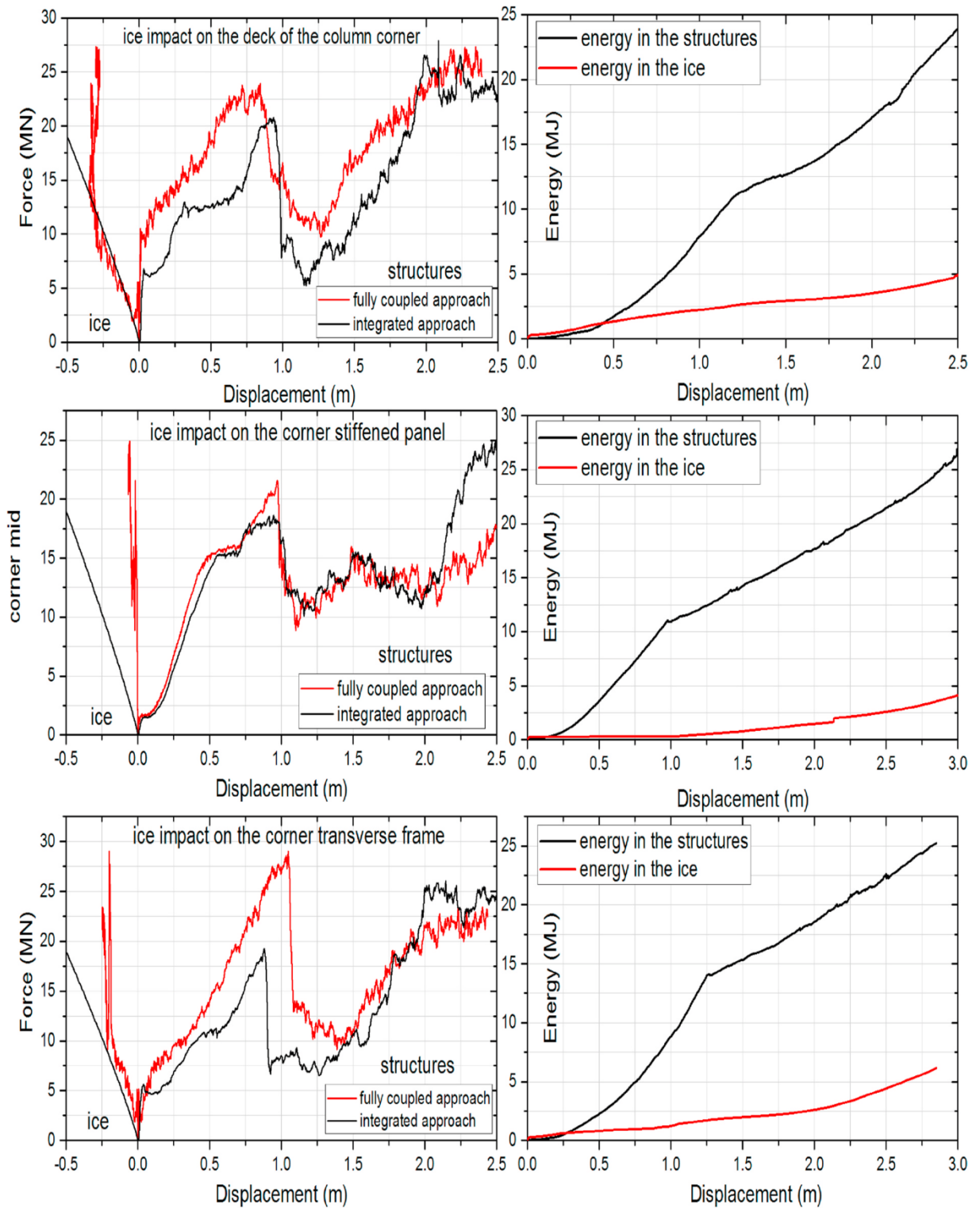
Fig. 30. (Left) Force displacement curves of the structure and ice for the ellipsoidal ice with 2a = 23 m that impacts the deck, transverse frame and middle of the column corner. Integrated approach means that either ice or structure is rigid. (Right) Energy dissipation in structure and ice from fully coupled analysis.
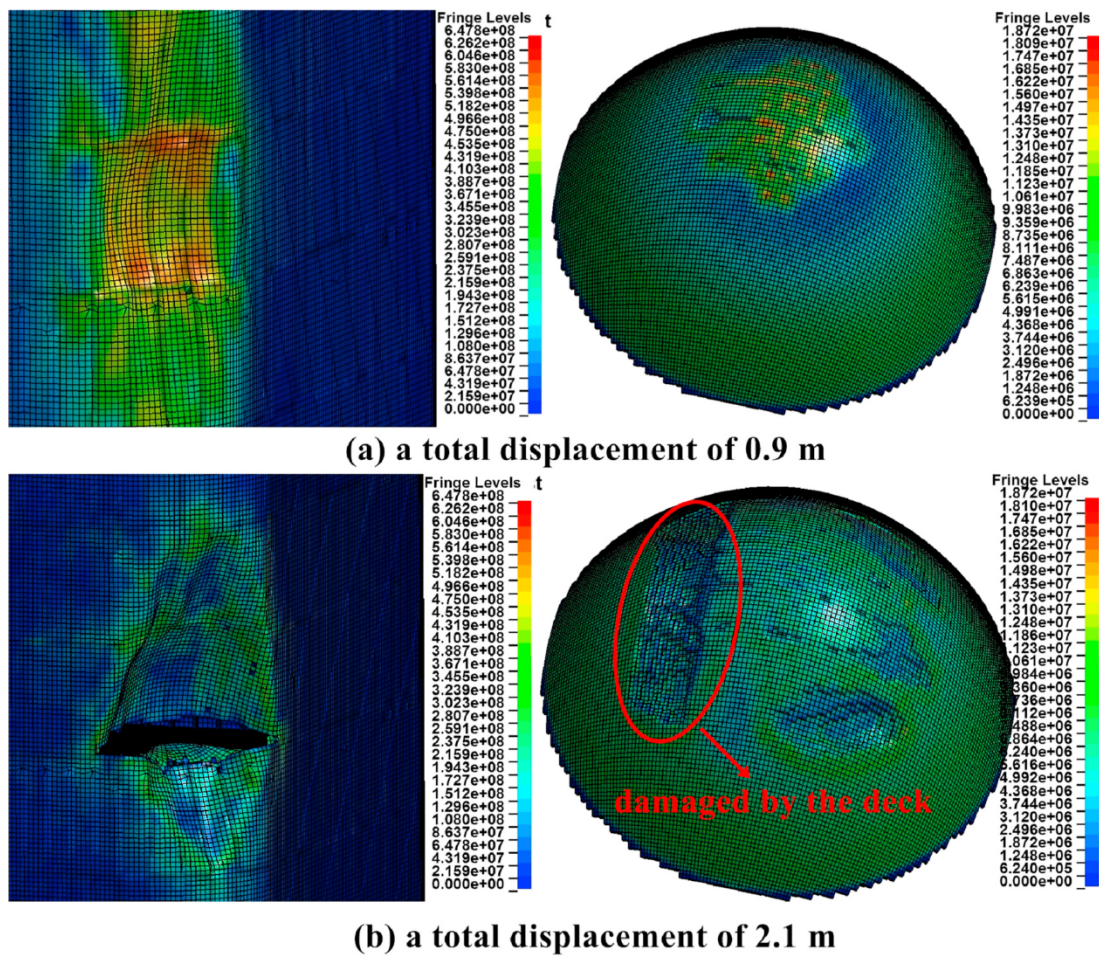
(a) a total displacement of 0.9 m

(b) a total displacement of 2.1 m

Fig. 31. Structural damage and ice crushing for ice impact on the corner stiffened panel.

ductile behaviour, which is pre-dominated by structural energy dissipation, to shared energy behaviour occurs. This transition occurs when the long axis of the ellipsoidal ice changes from 2a = 23 m to 2a = 30 m. The corresponding structural deformation decreases drastically during the transition. As the ice becomes even sharper, more energy is absorbed by ice crushing and the corresponding structural deformation decreases.

Impacts from blunt ice, i.e., ice with 2a ≤ 23 m, are more critical to the structure, which yields much larger structural energy absorption and structural deformation compared with impacts from sharp ice. Among all the blunt ice geometries, the ice with 2a = 23 m yields the largest structural deformation as the energy absorption capacity of a structure is closely related to the loading area. Given the same total energy, the largest structural deformation will be obtained for impacts from the least blunt ice with the smallest loading area provided that the ice is sufficiently blunt to avoid being crushed by the structure. Therefore, the critical ice geometry is the ice model with 2a = 23 m.

All the six ellipsoidal ice shapes with different levels of sharpness are capable of causing large structural deformations. The ice with 2a = 23 m is considered to be critical for the structure: this corresponds to a ratio of the ice radius of curvature to the stiffened panel length of 0.81. Note that the critical geometry of ice is sensitive to the calibrated ice pressure area relationship and dimensions of the investigated structure.

6.3. Discussion of the three approaches

Three approaches are adopted to conduct the ice impact analysis and ice-structure interactions. The fully coupled approach predicts the most realistic results but is computationally the most demanding. By selecting the maximum structural deformation as an indicator of structural damage, the damage predicted by the three methods is plotted in Fig. 27 with various sharpness levels for the striking ice and a total energy dissipation of 7.5 MJ. Two separate regions are identified. In the blunt ice region, the weakly coupled analysis yields results that are rather similar to the fully coupled analysis, whereas the integrated analysis seems to be less conservative. In the sharp ice region, where the ice is crushed significantly, both the weakly coupled analysis and integrated analysis appear to be too
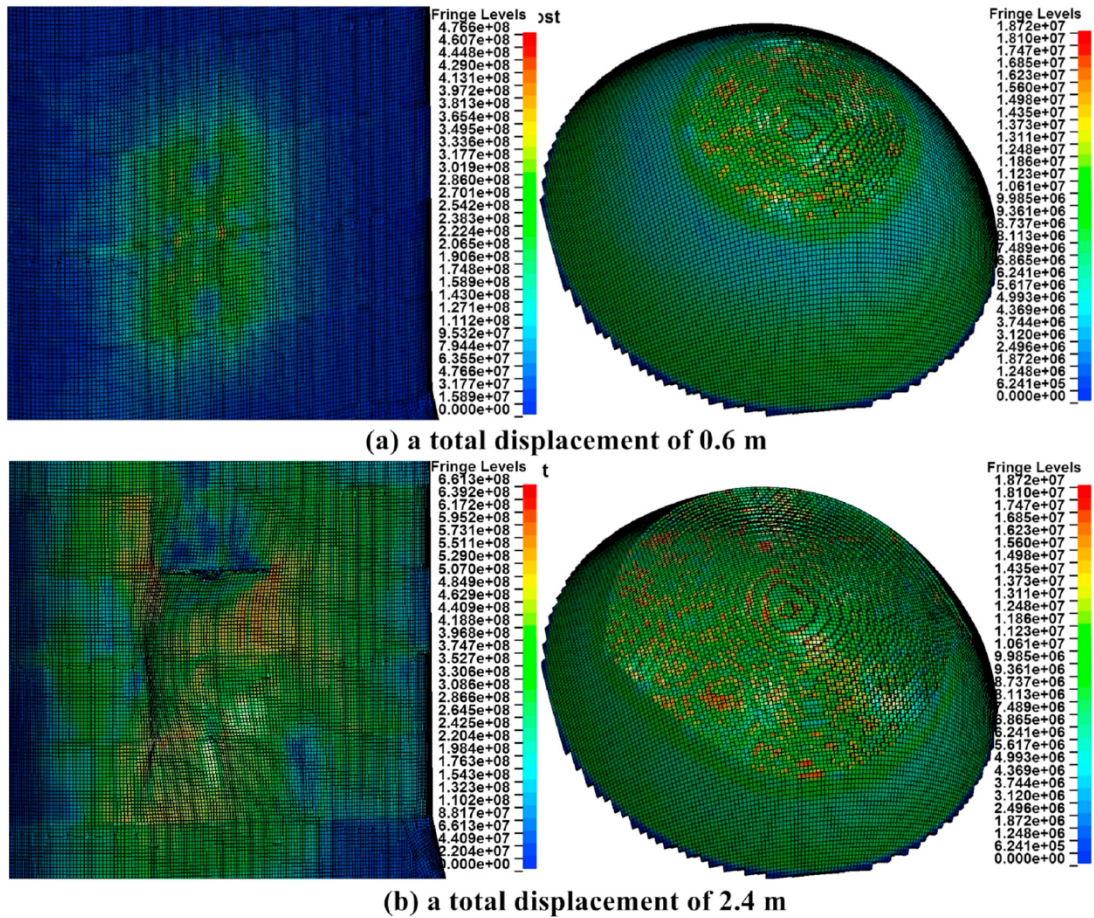
Fig. 32. Structural damage and ice crushing for ice impact on the cruciform of the column front.
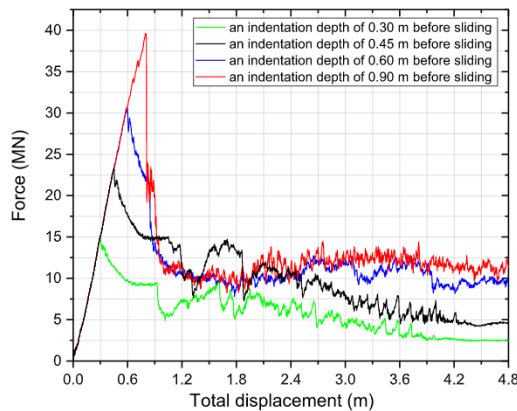

Fig. 33. Impact resistance curve for combined indentation and sliding ice loads.

conservative compared with the fully coupled analysis as they both substantially overestimate the structural deformation. In these conditions, the fully coupled approach should be employed.

In addition, the energy dissipation using the integrated approach and weakly coupled approach is calculated by integrating the force-deformation curves of the ice or structure, which is also adopted in ISO 19906 and IACS rules for ULS design, e.g., Daley [36]. However, this approach does not hold in ALS conditions, i.e. $E \neq \int F(\delta) \cdot d\delta$, where δ denotes the characteristic displacement of either the ice or the structure, as in ALS conditions, both the ice and the structure deform significantly and the displacement is not uniform on
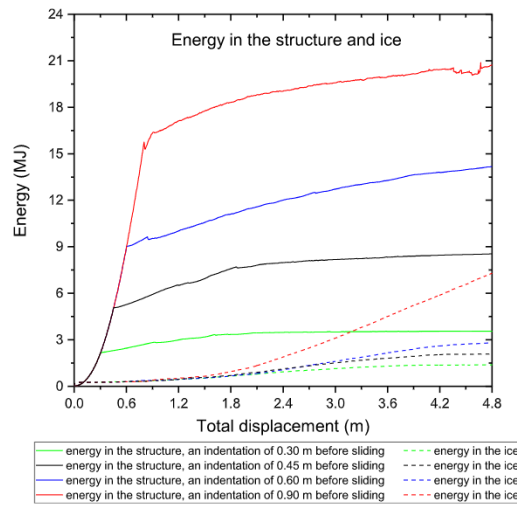
Fig. 34. Energy absorption in the structure and ice under combined indentation and sliding ice loads.

the contact plane but is a function of location. A representative characteristic displacement cannot be obtained in general. This represents another error source of the integrated approach and weakly coupled approach.

7. Analysis of structural response subjected to ice impacts with the critical sharpness

The ellipsoidal ice with 2a = 23 m and 2b = 2c = 10.4 m is determined to be critical with respect to penetration of the stiffened panel in Section 6.2. This ice geometry is adopted to collide with different locations of the platform column. The structural responses are analysed with the fully coupled approach and integrated approach, and the results are compared and discussed.

7.1. Response of the column structure to ice indentation

Fig. 28 (left) displays the force versus total displacement (including deformation of both ice and structure) at different impact locations of the platform column. The locations are defined in Fig. 28 (right). The curves show significant effects of ice-structure interaction, which do not follow the rigid ice-only curve or the rigid structure-only curve but follow a combination of both curves. Fig. 29 and Fig. 30 show separately the force deformation curves for the structure, ice and corresponding energy absorption. For the impacts on stiffened panels of the column front and column corner, the ice is very stiff and deforms the structures with minor ice damage, i.e., ductile behaviour. Outer shell fracture occurs at a total energy dissipation of 15 MJ for stiffened panels at the column front and a total energy dissipation of 11 MJ at the column corner. The structural damage and ice crushing for ice impacts on the column corner are given in Fig. 31. The ice is virtually rigid most of the time but is crushed to some extent when it makes contact with the stiffened deck.

For ice impacts on the bulkhead, the intersection between the bulkhead and the deck, corner deck and corner transverse frame, both the ice and the structure are damaged, and significant ice-structure interaction takes place. We consider the case of ice impacts on the intersection between the bulkhead and the deck (denoted as cruciform in Fig. 29) as an example. As indicated by the resistance curves in Fig. 29 and plots of structural damage and ice crushing in Fig. 32, the intersection between the bulkhead and the deck is very stiff initially and crushes the ice significantly. The ice crushing force curve follows perfectly the design ice resistance curve to a deformation of 0.6 m, beyond which the cruciform structure starts to collapse and deflect. After ice crushing of 0.6 m, both the ice and the structure deform and absorb energy. The structural deformation increases the contact area, and therefore, the ice resistance starts to deviate from the design ice curve. Simultaneously, the load carrying capacity of the structure increases with an increase in the contact area. A similar behaviour is also observed for ice impacts on the bulkhead, corner deck and corner transverse frame.

7.2. Response of column stiffened panels to ice moving loads

The simulations above consider mainly head-on ice impacts. However, oblique impacts occur often in reality, which will induce not only indentation in the normal direction but also sliding damage in the tangential plane. The ice loads associated with sliding along the structure are termed moving loads. The effects of moving loads were investigated by Alsos [37] for ship grounding and Quinton [38] for ice sliding.

The stiffened panel of the column front is selected for studying ice sliding damage on the structure with the identified critical ice geometry. An initial indentation depth of 0.30 m, 0.45 m, 0.60 m and 0.90 m is created before the ice starts to slide along the panel. Fig. 33 shows the resistance-displacement curves for the three cases. The displacement includes an initial indentation and the displacement for sliding along the panel. The corresponding energy dissipation in the ice and the structure is plotted in Fig. 34, and the
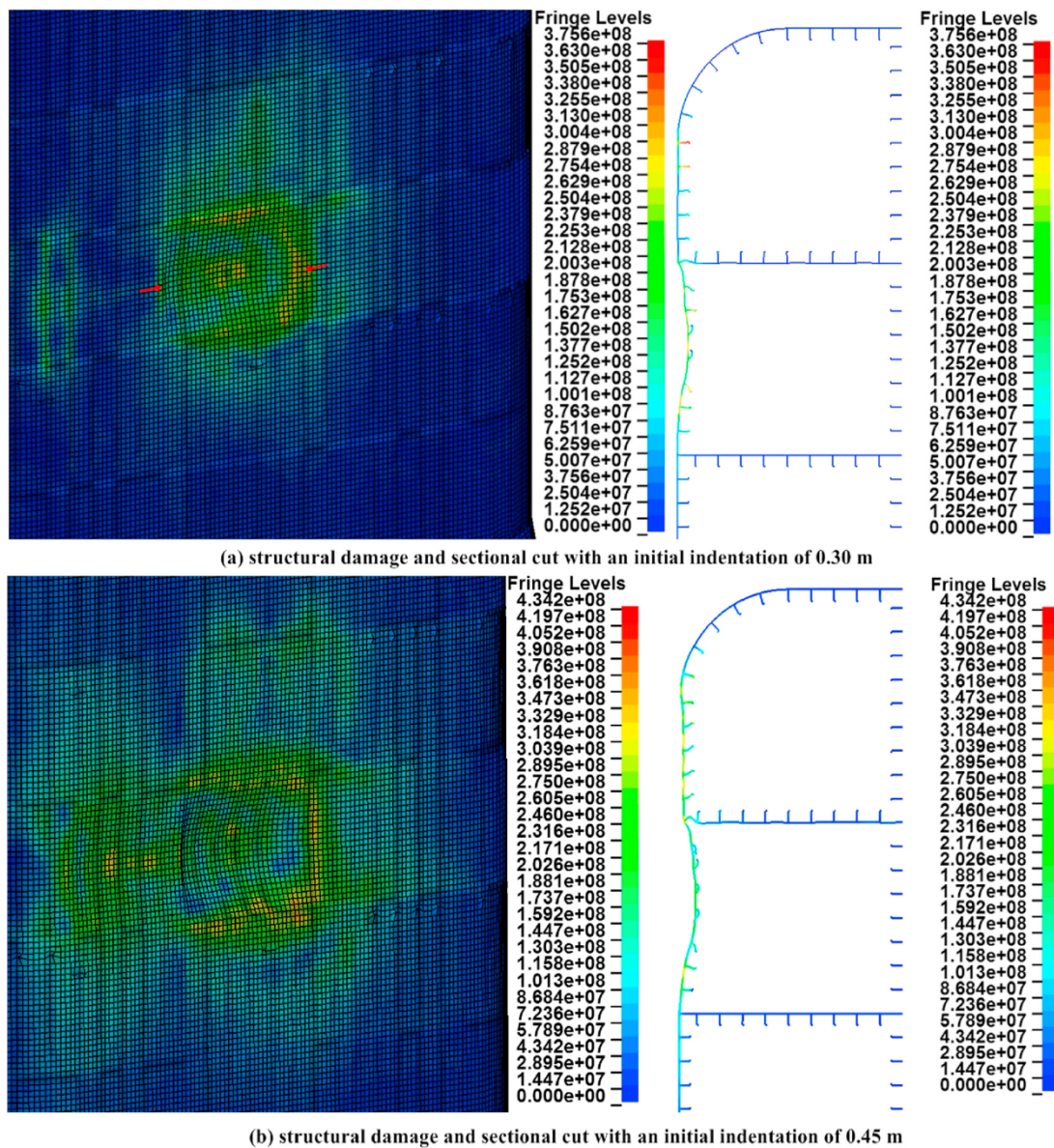
(a) structural damage and sectional cut with an initial indentation of 0.30 m

(b) structural damage and sectional cut with an initial indentation of 0.45 m

Fig. 35. Structural damage subjected to ice moving loads. The initial indentation depths before sliding are 0.30 m and 0.45 m.

structural damage for the three cases is shown in Fig. 35, Fig. 36 and Fig. 37.

The resistance drops drastically when the impact shifts from indentation to sliding, and then the force level tends to stabilize during continuous sliding. A shown in Fig. 34, a significantly lower slope of the structural energy curve is observed, which indicates a considerably reduced energy absorption capability of the structure to moving loads. For the case with an initial indentation of 0.30 m and 0.45 m, progressive damage occurs without outer shell fracture; refer to Fig. 35. The steady sliding resistance is virtually half the value of the indentation force, which is consistent with experimental findings by Quinton [38]. For the case with an initial indentation of 0.6 m and 0.9 m, the panel is continuously torn open (refer to Figs. 36 and 37) with a steady force level, and the tearing force is virtually the same. During the process, the ice is slightly damaged when sliding along the stiffened panel but becomes significantly crushed when it contacts the bulkhead (refer to Fig. 38). It is interesting to find that the sliding resistance for cases without shell fracture can exceed the resistance for cases with continuous tearing of the outer shell.

The sliding damage analysis reveals that a structure is more vulnerable to combined moving loads and indentation loads compared with cases with indentation loads only because moving loads with an initial structural indentation are capable of causing the same structural deformation with a considerably lower force level and significantly degrades the structural capability of energy absorption. During sliding, the panel undergoes biaxial stretching. Once an initial crack occurs, stress concentrations at the crack tip will easily cause continuous tearing of the panel and progressive collapse. The moving loads therefore require additional studies and should be
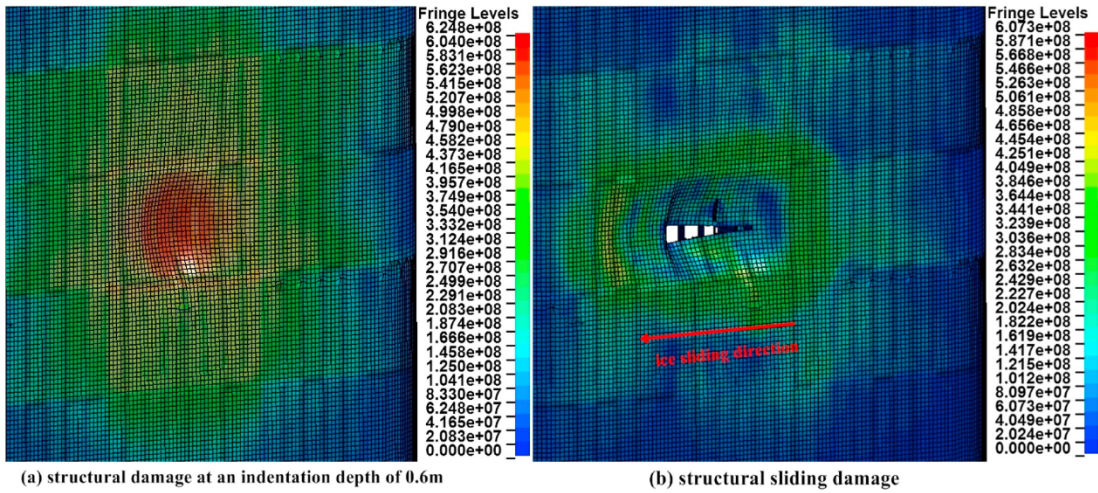
(a) structural damage at an indentation depth of 0.6m   (b) structural sliding damage

Fig. 36. Structural damage subjected to moving loads. The initial indentation depth before sliding is 0.60 m.

(a) structural damage at an indentation depth of 0.9m   (b) structural sliding damage
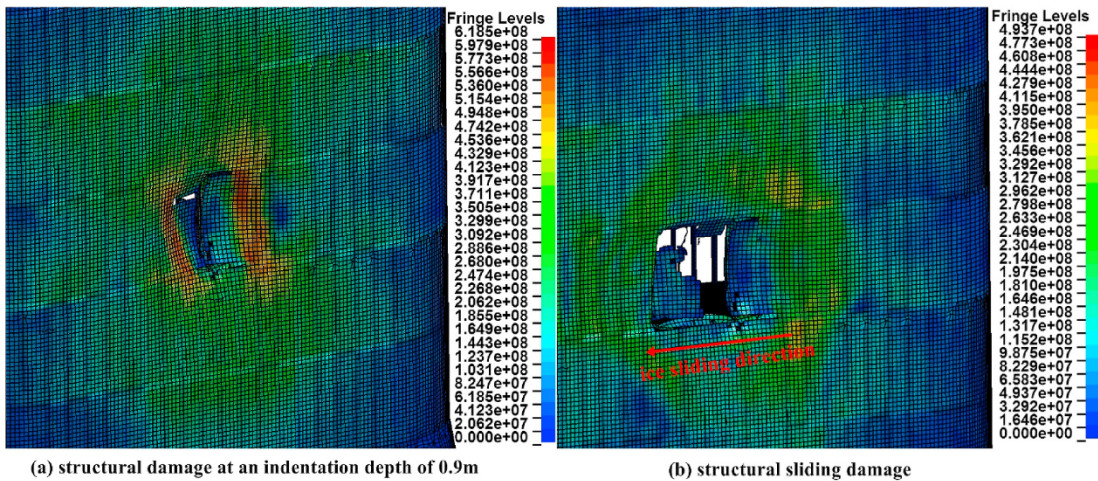
Fig. 37. Structural damage subjected to moving loads. The initial indentation depth before sliding is 0.90 m.
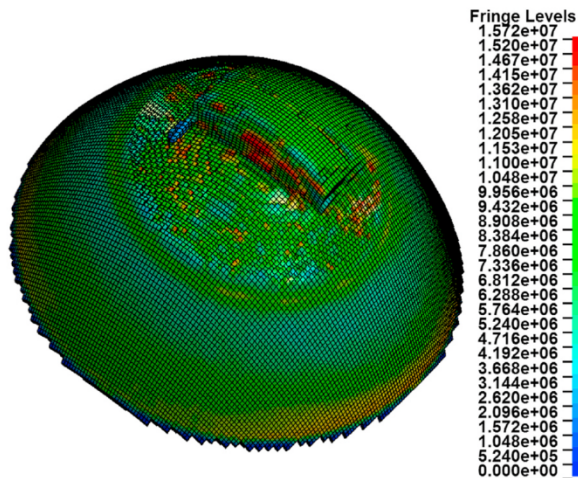

Fig. 38. Ice damage during sliding with an initial indentation depth of 0.90 m.

carefully considered in any design.

8. Conclusions

Paper II presents a damage assessment of an offshore semi-submersible platform column that is subjected to glacial ice impacts. Three different approaches were adopted with various degrees of simplifications, i.e., integrated approach, weakly coupled approach and fully coupled approach. The following conclusions are obtained:

1. An important finding is the existence of a critical local sharpness of ice, which causes the maximum structural damage for a given impact energy. The ice local geometry is described by the radius of curvature. The shapes with the smallest radius of curvature will be crushed, while the shapes with the largest radius of curvature will deform the platform with moderate ice crushing. The critical geometry is the radius of curvature that for a given impact energy maximizes the penetration of the installation. This geometry is based on the supposition that penetration that may cause flooding of empty compartments or spillage from cargo tanks is the critical outcome. If other failure modes are considered more relevant (e.g., residual strength of damaged members), the critical shape must be searched with respect to these criteria.

   From the fully coupled simulations, a critical ice sharpness for the given column stiffened panel is identified, where the ice radius of curvature is 0.81 times the stiffened panel length. It should be noted that the critical ice sharpness is closely related to the structural layout and material strength, as well as the selected pressure-area (P-A) relationship for the calibration of the ice material. The sensitivity of the critical ice sharpness and structural responses to these factors need to be studied further.

2. Significant ice-structure interaction is observed during glacial ice impacts in ALS conditions, where the deformation of both ice and the structure increases the actual contact area and the total resistance. The mutual interactions with the resistance of both bodies make it considerably different with the ULS scenarios, where the structure sustains minor damage with negligible interaction.
3. An elastic-plastic material model by Liu et al. [11] was employed to model the ice material in the fully coupled approach. The model assumes low speed impacts of glacial ice without considering any strain rate effect. The model was shown to be very sensitive to the mesh size with a strain-based failure criterion. To overcome this feature, calibration is recommended for each ice shape and element meshing. Two different ways exist to calibrate the design ice P-A curve, i.e., a deformable ice being crushed by a rigid panel and a rigid indenter being pushed into an ice block. The former is recommended because confinement models still lack validation, which yields conservative results.
4. The three different methods produce consistent predictions of structural damage in general; the results are complimentary to each other. Of the three methods, the fully coupled approach produces the most realistic results and is capable of simulating the complicated ice-structure interactions quite well. However, this approach is the most computationally demanding method. The weakly coupled and integrated approaches require little computation time and can be employed for a large number of simulations and subsequent probabilistic analysis. The weakly coupled approach is superior to the integrated approach because it captures the one-way coupling of structural deformation on the ice resistance.

   The integrated and weakly coupled approaches are most suitable for scenarios with blunt ice, where ice crushing is minor, as both methods do not update the structural F-D curve when ice undergoes damage. If the ice is significantly crushed, the contact area increases, which increases the structural capacity to ice loading but is not reflected in both methods. Therefore, in scenarios with sharp ice, the fully coupled method should be employed.

5. With the most unfavourable local ice geometry, current calculations indicate that the structure can withstand a maximum impact energy level of approximately 15 MJ. Therefore, a maximum impact energy of approximately 7.5 MJ identified from Paper I is considered safe to the structure. However, the lowest size limit of a detectable glacial ice feature can easily be doubled to 30 m according to Lu et al. [17]. Thus, a much higher impact energy may be expected, with concern for the structural safety.

Declaration of competing interest

The authors declare that they have no known competing financial interests or personal relationships that could have appeared to influence the work reported in this paper.

References

[1] ISO-19906. Arctic offshore structures standard. 2010.

[2] Amdahl J. Impact from ice floes and icebergs on ships and offshore structures in Polar Regions. 2nd Computational Methods in Offshore Technology; 2019. COTech 2019.

[3] Jordaan IJ. Mechanics of ice–structure interaction. Eng Fract Mech 2001;68(17–18):1923–60.

[4] Kõrgesaar M, Kujala P, Romanoff J. Load carrying capacity of ice-strengthened frames under idealized ice load and boundary conditions. Mar Struct 2018;58: 18–30.

[5] Yu Z, Amdahl J, Sha Y. Large inelastic deformation resistance of stiffened panels subjected to lateral loading. Mar Struct 2018;59:342–67.

[6] Daley CG, Daley KH, Dolny J, Quinton BW. Overload response of flatbar frames to ice loads. Ships Offshore Struct 2017;12(sup1):S68–81.

[7] Gagnon R. A numerical model of ice crushing using a foam analogue. Cold Reg Sci Technol 2011;65(3):335–50.

[8] Gagnon R, Wang J. Numerical simulations of a tanker collision with a bergy bit incorporating hydrodynamics, a validated ice model and damage to the vessel. Cold Reg Sci Technol 2012;81:26–35.

[9] Fish AM. Creep and yield model of ice under combined stress. COLD REGIONS RESEARCH AND ENGINEERING LAB HANOVER NH; 1991.

[10] Derradji-Aouat A. A unified failure envelope for isotropic fresh water ice and iceberg ice. 2000.

[11] Liu Z, Amdahl J, Løset S. Plasticity based material modelling of ice and its application to ship-iceberg impacts. Cold Regions Science and Technology; 2011.

[12] Xu Y, Hu Z, Ringsberg JW, Chen G. Nonlinear viscoelastic-plastic material modelling for the behaviour of ice in ice-structure interactions. Ocean Eng 2019;173: 284–97.

[13] Ince ST, Kumar A, Paik JK. A new constitutive equation on ice materials. Ships Offshore Struct 2017;12(5):610–23.

[14] Ince ST, Kumar A, Park DK, Paik JK. An advanced technology for structural crashworthiness analysis of a ship colliding with an ice-ridge: numerical modelling and experiments. Int J Impact Eng 2017;110:112–22.

[15] Cai W, Zhu L, Yu T, Li Y. Numerical simulations for plates under ice impact based on A concrete constitutive ice model. Int J Impact Eng 2020:103594.

[16] Han D, Lee H, Choung J, Kim H, Daley C. Cone ice crushing tests and simulations associated with various yield and fracture criteria. Ships Offshore Struct 2017; 12(sup1):S88–99.

[17] Lu W, Yu Z, Marnix VdB, Dennis M, Raed L, Vegard H, Amdahl J, Løset S, Kim E. Loads, design and operations of floaters in the arctic (nord ST20). 2019. PTIL - LASTER, DESIGN OG OPERASJON AV FLYTERE I NORDOMRÅDENE (NORD ST20) 2019/313.

[18] Lu W, Yu Z, Van den Berg M, Lubbad R, Amdahl J, Løset S, Kim E. Assessment of structural damage due to glacial ice impact. Petroleumstilsynet, Stavanger: PTIL-Konstruksjonssikkerhet i Nordområdene; 2018.

[19] Ommani B, Berthelsen PA, Firoozkoohi R. OC2018 A-116-Loads, design and operation of floaters in the Arctic-Ptil–NORD ST20. 2018.

[20] ARCISO. Arctic integrated solutions with the simulator for arctic marine structures (SAMS). 2020. https://arciso.com/.

[21] Lu W, Amdahl J, Lubbad R, Yu Z, Løset S. Glacial ice impacts, Part I: wave-driven motion and small glacial ice feature impacts. 2020 [Submitted to jounal].

[22] Kennedy KP. Dynamic activity and crushed ice behavior in medium-scale ice-structure interactions. Memorial University of Newfoundland; 1990.

[23] Daley C. MSI ice loads data: compilation of medium scale ice indentation test results and comparison to ASPPR. Daley R & E; 1994.

[24] IACS. Requirements concerning polar class. International Association of Classification Societies London; 2011.

[25] Dnv-RP-C204. Recommended practice DNV-RP-C204. DET NORSKE VERITAS; 2019.

[26] ISO19906. Petroleum and natural gas industries – Arctic offshore structures. International Organization for Standardization; 2010.

[27] Timco GW, Weeks WF. A review of the engineering properties of sea ice. Cold Reg Sci Technol 2010;60(2):107–29.

[28] Kierkegaard H. Ship collisions with icebergs. Danmarks tekniske højskole, instituttet for skibs-og havteknik. 1993.

[29] Tavakoli MT, Amdahl J. Analysis of collision between Midgard platform and 8000 tonnes displacement ship. 2010.

[30] Alsos HS, Hopperstad OS, Törnqvist R, Amdahl J. Analytical and numerical analysis of sheet metal instability using a stress based criterion. Int J Solid Struct 2008;45(7):2042–55.

[31] Hill R. On discontinuous plastic states, with special reference to localized necking in thin sheets. J Mech Phys Solid 1952;1(1):19–30.

[32] Bressan J, Williams J. The use of a shear instability criterion to predict local necking in sheet metal deformation. Int J Mech Sci 1983;25(3):155–68.

[33] Marinatos JN, Samuelides MS. Material characterization and implementation of the RTCL, BWH and SHEAR failure criteria to finite element codes for the simulation of impacts on ship structures, 6th International Conference on Collision and Grounding of Ships and Offshore Structures. Trondheim: ICCGS 2013; 2013. p. 57–67.

[34] Storheim M, Amdahl J, Martens I. On the accuracy of fracture estimation in collision analysis of ship and offshore structures. Mar Struct 2015;44:254–87.

[35] EKEBERG O-C, Shipilova O, Birknes-Berg Johansen J. Glacial ice impact. PTIL - KONSTRUKSJONSSIKKERHET I ARKTISKE OMRÅDER (ST5) DNV GL; 2017.

[36] Daley C. Energy based ice collision forces. Proceedings of the 15th international conference on port and ocean engineering under arctic conditions (POAC). 1999. p. 674–86.

[37] Alsos HS. Ship grounding: analysis of ductile fracture, bottom damage and hull girder response. 2008.

[38] Quinton BW. Progressive damage to a ship's structure due to ice loading. Memorial University of Newfoundland; 2008.